

# Gravity field models from kinematic orbits of CHAMP, GRACE and GOCE satellites

Aleš Bezděk<sup>a,\*</sup>, Josef Sebera<sup>a</sup>, Jaroslav Klokočník<sup>a</sup>, Jan Kostelecký<sup>b</sup>

<sup>a</sup>Astronomical Institute, Academy of Sciences of the Czech Republic, Fričova 298, 251 65 Ondřejov, Czech Republic

<sup>b</sup>Research Institute of Geodesy, Topography and Cartography, Ústecká 98, 250 66 Zdíby, Czech Republic

---

## Abstract

The aim of our work is to generate Earth's gravity field models from GPS positions of low Earth orbiters. Our inversion method is based on Newton's second law, which relates the observed acceleration of the satellite with forces acting on it. The observed acceleration is obtained as numerical second derivative of kinematic positions. Observation equations are formulated using the gradient of the spherical harmonic expansion of the geopotential. Other forces are either modelled (lunisolar perturbations, tides) or provided by onboard measurements (nongravitational perturbations). From this linear regression model the geopotential harmonic coefficients are obtained.

To this basic scheme of the *acceleration approach* we added some original elements, which may be useful in other inversion techniques as well. We tried to develop simple, straightforward and still statistically correct model of observations. (i) The model is *linear* in the harmonic coefficients, *no a priori* gravity field model is needed, no regularization is applied. (ii) We use the *generalized least squares* to successfully mitigate the strong amplification of noise due to numerical second derivative. (iii) The number of other fitted parameters is very small, in fact we use only daily biases, thus we can monitor their behaviour. (iv) GPS positions have correlated errors. The sample autocorrelation function and especially the *partial autocorrelation function* indicate suitability of an autoregressive model to represent the correlation structure. The *decorrelation of residuals* improved the accuracy of harmonic coefficients by a factor of 2–3. (v) We found it better to compute separate solutions in the three local reference frame directions than to compute them together at the same time; having obtained separate solutions for along-track, cross-track and radial components, we combine them using the normal matrices. Relative contribution of the along-track component to the combined solution is 50 percent on average. (vi) The computations were performed on an ordinary PC up to maximum degree and order 120.

We applied the presented method to orbits of CHAMP and GRACE spanning seven years (2003–2009) and to two months of GOCE (Nov/Dec 2009). The obtained long-term static gravity field models are of similar or better quality compared to other published solutions. We also tried to extract the *time-variable gravity* signal from CHAMP and GRACE orbits. The acquired average annual signal shows clearly the continental areas with important and known hydrological variations.

**Keywords:** Gravity field models, Kinematic orbits, Generalized least squares, Partial autocorrelation function, Time-variable gravity

---

## 1. Introduction

In the 'Decade of the geopotential' (2000–2010) three major satellite missions were launched with the aim to significantly improve the global gravity field model of the Earth.

In 2000 the German satellite CHAMP (CHALLENGING Minisatellite Payload) was put in a 450-km orbit inclined at 87.3° (Reigber et al., 2002). It was a realization of the concept called *satellite-to-satellite tracking in the high-low mode* (GPS-SST): A low Earth orbiter is tracked by high orbiting GPS satellites, relative to a net of ground stations. Nongravitational forces acting on the low orbiter are measured by an onboard accelerometer (Rummel, 2002). The use of an onboard geodetic-quality GPS receiver and efficient postprocessing provided a long series of precise 3-D positions with constant time step. CHAMP proved that GPS-SST is a very effective technique for global gravity field mapping; already the first CHAMP models improved the pre-CHAMP satellite-only models by an order of magnitude in low

degrees (Reigber et al., 2003a). The CHAMP satellite decayed from its orbit in 2010.

The German/US GRACE mission (Gravity Recovery And Climate Experiment), launched in 2002, consists of two satellites freely decaying from an initial 500-km orbit inclined at 89° (Tapley et al., 2004). In this way the concept of *satellite-to-satellite tracking in the low-low mode* was first realized. The relative motion between the GRACE A and GRACE B satellites following each other in the same orbit at a distance of 220 km is measured by *K-band microwave ranging* (KBR). The technique of satellite-to-satellite tracking based on GRACE KBR data currently yields the best global gravity fields at low to medium degrees (Tapley et al., 2007; Mayer-Gürr et al., 2010). The GRACE mission has launched a new era in studying time-variations of Earth's gravity field observed from space (for recent review of results, see e.g. Cazenave and Chen, 2010; Chambers and Schröter, 2011).

Finally, in 2009 the European Space Agency launched GOCE (Gravity Field and Steady-State Ocean Circulation Explorer), a satellite carrying the first space gradiometer, to a sun-synchronous orbit with an inclination of 96.7° (ESA, 1999; Floberghagen et al., 2011). In *satellite gravity gradiometry*

---

\*Corresponding author

Email addresses: bezdek@asu.cas.cz (Aleš Bezděk), sebera@asu.cas.cz (Josef Sebera), jklokocn@asu.cas.cz (Jaroslav Klokočník), kost@fsv.cvut.cz (Jan Kostelecký)

(SGG), the second-order derivatives of the Earth gravitational potential are measured by a low orbiting satellite using differential accelerometry (Rummel, 2002). The extremely low GOCE observation altitude of 255 km and less is enabled by the action of an onboard ion thruster (drag-free control), which successfully compensates for the atmospheric drag. The gravity fields from SGG should be best at medium to high degrees, which is indeed the case (Pail et al., 2011a). The noise characteristics of the GOCE gradiometer does not allow its data to be used for the accurate recovery of the low-degree harmonics of the gravity field. For this purpose an onboard GPS receiver is used, and the full GOCE gravity fields are obtained by combining data from the GPS-SST and SGG techniques.

The primary motivation behind the study presented in this paper was to compute a gravity field model up to say degree 70 through inversion of satellite orbits (Bezděk et al., 2012). With the availability of precise kinematic positions from the continuous GPS tracking of CHAMP (Švehla and Rothacher, 2005; Švehla and Földváry, 2006), new computational approaches emerged (Reigber et al., 2003b; Reigber et al., 2005b). From these we chose the acceleration approach, which we subsequently modified. In connection with the launch of the CHAMP mission, the general idea of the acceleration approach was proposed and discussed by several authors (e.g. Reubelt et al., 2003, 2006; Götzelmann et al., 2006; Ditmar and Sluijs, 2004; Sluijs, 2002; Schäfer, 2000). The acceleration approach has a number of interesting features: it is conceptually very simple, it produces a linear regression system for the unknown geopotential coefficients (no linearization is necessary), all three GPS position components are used, in principle it could be treated on an ordinary personal computer. It was estimated that the gravity field models from the GRACE KBR data would be two orders of magnitude more accurate in low degrees compared to models based on GPS-SST (ESA, 1999; Rummel, 2002). The current KBR models are indeed superior, recent ITG-Grace2010S model (Mayer-Gürr et al., 2010) has half the GPS/levelling error compared to the GPS-SST model AIUB-CHAMP03S (Prange, 2010), as can be seen in the evaluation section of the ICGEM website (<http://icgem.gfz-potsdam.de/ICGEM/>). But the evaluation results depend a lot on the maximum degree used, Jäggi et al. (2011a) show that the validation results are virtually the same for these two models, when the harmonic coefficients up to degree 60 are used. Geographical maps of time-variable gravity show clearly that the accuracy of KBR monthly fields is at least 10 times better compared to monthly solutions from GPS-SST. However, it is of great use to be able to compute orbit-based gravity field models as accurately as possible. Nowadays the majority of low Earth orbiters are standardly equipped with onboard GPS receivers which might provide valuable data for gravity field modelling. The combination of precise orbital data from many such missions suitable for the inversion into harmonic coefficients would certainly be profitable for the static geopotential models, perhaps even more for studying the time-variable gravity. Monitoring temporal gravity field variations with the KBR technique may not be possible for some time, if the GRACE mission fails prior to the launch of its follow-on mission; in that case, GPS-SST data, as those from the Swarm mission to be launched by ESA in 2013 (ESA, 2004), may serve as a source of informa-

tion about the time-varying gravity field. Besides, Gunter et al. (2011) recently showed that a constellation of several tens of low-Earth satellites equipped with GPS receivers might possibly complement and reinforce a GRACE-like mission.

The purpose of this paper is to present our method in detail (Section 2) and the first results obtained (Section 3). Readers, who may want to avoid the technical and implementation details of the method, could skip Sections 2.2–2.5 and go directly to Section 3 with the results. These include the static and time-variable gravity field models from CHAMP and GRACE A/B orbits, and first results for GOCE. In Section 4 conclusions and outlook will be given. Our yearly and multi-year geopotential solutions together with their full covariance matrices are available for download at <http://www.asu.cas.cz/~bezdek/vyzkum/geopotencial/>.

## 2. Method

### 2.1. Linear regression model

For global gravity field analysis, the geopotential  $V$  at the point with spherical coordinates (radius  $r$ , co-latitude  $\theta$ , longitude  $\lambda$ ) is represented in spherical harmonics up to degree  $N$  as

$$V(r, \theta, \lambda) = \frac{GM}{r} \sum_{n=0}^N \left(\frac{R}{r}\right)^n \sum_{m=0}^n P_{nm}(\cos \theta) [C_{nm} \cos m\lambda + S_{nm} \sin m\lambda] \quad (1)$$

where  $GM$  is the geocentric gravitational constant,  $R$  the Earth's equatorial radius,  $P_{nm}$  the fully normalized associated Legendre functions of degree  $n$  and order  $m$ ,  $C_{nm}$  and  $S_{nm}$  the geopotential harmonic coefficients. For later reference, we will rewrite the geopotential harmonic series (1) in a shorter form

$$V(\mathbf{r}) = \sum_{n,m} [C_{nm} V_{nm}^{(c)}(\mathbf{r}) + S_{nm} V_{nm}^{(s)}(\mathbf{r})] \quad (2)$$

to explicitly show its linearity in the harmonic coefficients  $C_{nm}$  and  $S_{nm}$ .

The so-called acceleration approach is based on Newton's second law, which relates the forces acting on a body and its motion caused by these forces. Expressed in accelerations for a satellite in low Earth orbit, we will use Newton's second law in the form

$$\frac{d^2 \mathbf{r}}{dt^2} = \mathbf{a}_{\text{grav}} + \mathbf{a}_{\text{LS}} + \mathbf{a}_{\text{TID}} + \mathbf{a}_{\text{REL}} + \mathbf{a}_{\text{NG}}, \quad (3)$$

where  $\mathbf{r}$  is the position vector of the centre of mass of the satellite, and the terms on the right-hand side reflect the force vectors acting on the satellite:  $\mathbf{a}_{\text{grav}}$  gravitational acceleration due to the geopotential,  $\mathbf{a}_{\text{LS}}$  (direct) lunisolar perturbations,  $\mathbf{a}_{\text{TID}}$  acceleration due to solid Earth and ocean tides,  $\mathbf{a}_{\text{REL}}$  correction due to general relativity,  $\mathbf{a}_{\text{NG}}$  nongravitational accelerations. Now we rearrange the terms in Eq. (3) to yield the regression model.

We numerically approximate the second derivative of the position vector  $\mathbf{r}$  by double differentiation of GPS positions  $\mathbf{r}_{\text{gps}}$ . We do this by using polynomial smoothing filters. A polynomial  $Q$  of a chosen order is least-squares fitted to the data points within a running window; the approximate second derivative of  $\mathbf{r}$  at the

central point of the window is obtained by the differentiation of the fitted polynomial

$$d^2\mathbf{r}/dt^2 \approx d^2Q(\mathbf{r}_{\text{gps}})/dt^2 \equiv F * \mathbf{r}_{\text{gps}} . \quad (4)$$

For later reference, we will symbolically write the filtering of positions as the convolution of the second-derivative filter  $F$  and the radius-vector  $\mathbf{r}_{\text{gps}}$ . More about choosing the polynomial filters will be in Sect. 2.2.

The gravitational acceleration  $\mathbf{a}_{\text{grav}}$  is interpreted as the gradient of the geopotential  $V(\mathbf{r})$  as given in Eqs. (1) or (2)

$$\mathbf{a}_{\text{grav}}(\mathbf{r}) = \nabla V(\mathbf{r}) = \sum_{n,m} \left[ C_{nm} \nabla V_{nm}^{(c)} + S_{nm} \nabla V_{nm}^{(s)} \right] . \quad (5)$$

The lunisolar acceleration  $\mathbf{a}_{\text{LS}}$ , the acceleration  $\mathbf{a}_{\text{TID}}$  due to the solid Earth and ocean tides, and the relativistic corrective term  $\mathbf{a}_{\text{REL}}$  are all computed using the recent models (Sect. 2.5). For the nongravitational accelerations  $\mathbf{a}_{\text{NG}}$  we use observations from the onboard accelerometers. We will denote these accelerations by

$$\mathbf{a}_{\text{other}} \equiv (\mathbf{a}_{\text{LS}} + \mathbf{a}_{\text{TID}} + \mathbf{a}_{\text{REL}} + \mathbf{a}_{\text{NG}}) \quad (6)$$

and give more details about their treatment in Sect. 2.5.

*Linear regression model* — Substituting Eqs. (4)–(6) into (3), we obtain the observation equation

$$\frac{d^2Q(\mathbf{r}_{\text{gps}})}{dt^2} - \mathbf{a}_{\text{other}} = \sum_{n,m} \left[ C_{nm} \nabla V_{nm}^{(c)} + S_{nm} \nabla V_{nm}^{(s)} \right] + \varepsilon . \quad (7)$$

We obtain the harmonic coefficients  $C_{nm}$  and  $S_{nm}$  by solving the regression model, where one observation equation (7) is given at each GPS position of the satellite. There, the unknown harmonic coefficients  $C_{nm}$  and  $S_{nm}$  are linearly connected to the observed acceleration  $d^2Q(\mathbf{r}_{\text{gps}})/dt^2 - \mathbf{a}_{\text{other}}$ . We assume the term  $\mathbf{a}_{\text{other}}$  to have negligible uncertainty compared to that originating in GPS positions, therefore we treat  $\mathbf{a}_{\text{other}}$  as a deterministic vector (i.e. a vector not having a random component). The stochastic error  $\varepsilon$  represents the GPS-position observation error propagated to the acceleration domain. Equation (7) is linear in  $C_{nm}$  and  $S_{nm}$ , hence no a priori gravity field model is needed and the sought harmonic coefficients  $C_{nm}$  and  $S_{nm}$  could be obtained directly in one step using the ordinary least squares. The rest of Sect. 2 will be devoted to the discussion of numerical difficulties involved in this seemingly straightforward scheme. As mentioned in the introduction, readers interested in the results obtained from real data may omit the technical and implementation details of the presented method at first reading and may now go directly to Sect. 3.

Here we add a note explaining the choice of observation equations (7) in the domain of accelerations. The common way of solving the differential equations like the Newton law (3) is by integration. This is especially true in analytical treatment. In our study, we are provided with the observed precise positions. We can apply numerical differentiation to obtain a vector of observed accelerations (4). In our preceding paper (Bezděk, 2010), we found out that polynomial differentiation is a sort of Taylor series, which enables one to choose more or less arbitrarily the level of approximation of the numerical second derivative, the

level is set by the objective of the research. Advantage of having the observational equations (7) in the acceleration domain is that we may easily apply the same filter to the columns of the design matrix (and also to the vector  $\mathbf{a}_{\text{other}}$ ). Thus even if the signal is somewhat distorted by the approximate derivative, exactly the same distortion is applied to the basis functions (columns of design matrix). Also as regards other modelled acceleration terms  $\mathbf{a}_{\text{other}}$ , Eq. (6), it is easy to compute their point-wise values as acceleration vectors, but it would probably be more difficult to treat their numerically integrated values along the orbit. In this way, a linear regression system of equations for unknown geopotential coefficients, Eq. (7), was obtained in the acceleration domain.

In Sect. 2.2 we will discuss the choice of parameters for the polynomial filter of the numerical second derivative. Numerical differentiation of observational data containing random component (noise) usually has an unfortunate consequence in amplifying the noise and making it autocorrelated. Sect. 2.3 is devoted to the mitigation of these two unwanted effects. In this section, we suppose that the noise in the simulated GPS positions is uncorrelated normally distributed and that the only source of correlation of noise in the derived accelerations is the second-derivative filter. We show that it is possible to find a linear transformation matrix, whose application to the regression system (7) makes the random component of the observations again uncorrelated. After applying the linear transformation matrix to the regression system (7), we call it the ‘once-transformed’ model. In Sect. 2.4 real satellite GPS positions are introduced in the method development, they are input to the ‘once-transformed’ linear system and the model parameters are fitted. We show that the observation residuals are correlated, when real GPS positions are used as observations. Again, it is possible to find a linear transformation matrix that makes the random component of the observations approximately uncorrelated. To find the transformation matrix we make use of the covariance matrix of an estimated autoregressive process. We apply the linear transformation matrix and we call the new model ‘twice-transformed’. We show that for real observations the residuals of the ‘twice-transformed’ regression model are approximately uncorrelated normally distributed. This is the final form of our regression model, now we can be more confident in using statistical inference (e.g. error bars, covariances) about the estimated geopotential coefficients. Finally, in Sect. 2.5 other implementation details are presented.

## 2.2. Numerical approximation of second derivative

In Eq. (4) we introduced the polynomial filter  $d^2Q(\mathbf{r}_{\text{gps}})/dt^2$  as an approximation of second derivative of the satellite orbit  $d^2\mathbf{r}/dt^2$ . Here we use a FIR digital filter (finite impulse response filter), an analogy to the operation of moving average, where each data value is replaced by a linear combination of the data value and some number of its nearby neighbours. The idea of *polynomial smoothing filters*, also called *Savitzky-Golay filters*, is to approximate the underlying function within the moving window not by a constant (whose estimate is the average), but by a polynomial (Press et al., 2001, p. 644). The polynomial  $Q_k$  is of order  $k$  higher than one, typically quadratic or quartic, for derivatives usually  $k=4$  or larger is taken (ibid, p. 645). For a given window length  $w$ , polynomial order  $k$  and order of the derivative required, the filter coefficients are a set of constants. To preserve

the phase of the input signal, we take  $w$  to be odd and we assign the filter output value to the central point of the window. By its definition, the polynomial filter necessarily smoothes the studied geopotential signal; it is possible to take this smoothing into account easily, by applying the same filter (but only as a polynomial smoothing, without taking the second derivative of the polynomial coefficients) to the columns of the design matrix and to the deterministic vector  $\mathbf{a}_{\text{other}}$ .

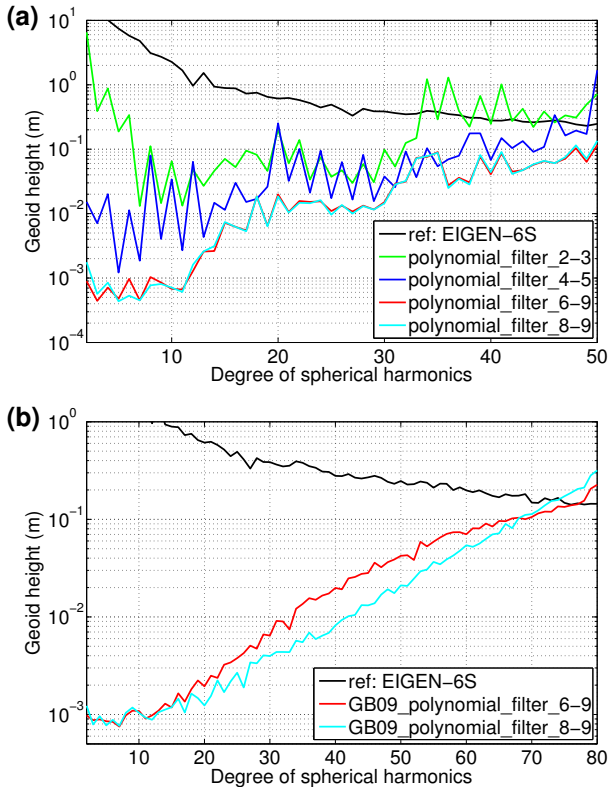


Figure 1: Degree difference amplitudes between the estimated and known harmonic coefficients. Example of experiments for choosing the optimum parameters  $k$ - $w$  of the second-derivative filter  $F$  ('polynomial\_filter\_ $k$ - $w$ '). In the upper panel we show the recovery for simulated orbits, in the lower panel for real orbits of GRACE B in 2009.

In order to find the optimum values  $k$  and  $w$  for the second-derivative polynomial filter  $F$ , we applied our inversion method to simulated orbits computed with a known gravity field model. To the simulated positions we added noise with different characteristics (white or correlated noise, different values of its variance). We evaluated the success of the recovery of the original harmonic coefficients using different criteria, e.g. the average or median difference as a function of the order. In the upper panel of Fig. 1 the results of a series of such experiments are shown in terms of degree difference amplitudes (Sect. 3.4). It is evident that the quality of the recovery depends a lot on the chosen pair of values  $k$  and  $w$ . The best two results using the simulated orbits correspond to the filters with the  $k$ - $w$  parameters 6-9 and 8-9. In the lower panel of Fig. 1 these two filters are applied to one year of GRACE B data. Using *real* positions, the resulting yearly solutions are different, clearly the filter 8-9 performs better, probably because of systematic errors, which were not well represented in the *simulated* orbits.

For choosing the optimum  $k$ - $w$  filter parameters we tested many configurations using the simulated and real orbits. Finally, for the 10-sec CHAMP orbits we selected the best pairs 6-9 and 6-15, for the 30-sec GRACE A/B orbits the pair 8-9, for the 1-sec GOCE orbit the 4-19 pair of the filter parameters. Different results for individual satellites are caused mainly by different orbit sampling. (The choice of the reference gravity field model, which we used when working with real orbits, is discussed in Sect. 3.4.)

Press et al. (2001, p. 644) characterize Savitzky-Golay filters as low pass filters, and as such their defining parameters have impact on their action in the frequency domain. In accordance with the examples in Press et al. (2001), our experience is that the choice of the filter parameters, especially its order, has a significant influence on what frequency content is preserved by applying the filter to the signal in question. The specific pair 8-9 of filter parameters is in accordance with the results of other groups (e.g., Baur et al., 2012).

Estimating the gravity field models from real data is a rather complex procedure and every method has a certain number of intrinsic defining parameters. The purpose of this subsection was to show that the chosen values of intrinsic parameters may be of primary importance for the results obtained, even if the method itself is comparable in its definition to other inversion methods. In case of the acceleration approach and in the framework of computing the longwave portion of the GOCE geopotential models from GPS-SST data, recently there appeared several publications dealing with similar problems, each having specific and sometimes somewhat different conclusions regarding the methodology and optimum parameters (Baur et al., 2012; Zehentner et al., 2012; Reubelt et al., 2012; Weigelt et al., 2011; Reubelt et al., 2003).

### 2.3. Problem of noise amplification due to second derivative

It is common in scientific applications to have to calculate the derivative of a function specified by experimental data, which is corrupted by noise. Practitioners know that calculating numerical derivatives will amplify this noise, often so much that the result is useless. This general rule unfortunately applies to the orbit inversion as well, even for the first derivative of GPS positions used in the energy balance approach the noise amplification problem has to be treated carefully (Weigelt and Sneeuw, 2005). For double differentiation the amplification of noise is even worse, this can be seen by using a Fourier transform pair (Press et al., 2001, p. 490)

$$h(t) \iff H(f) = \int_{-\infty}^{+\infty} h(t)e^{2\pi if t} dt, \quad (8)$$

where  $h(t)$  is a time-domain function and  $H(f)$  its frequency-domain counterpart. The  $n^{\text{th}}$  derivative in the time domain has the transform

$$h^{(n)}(t) \iff (2\pi if)^n H(f) \quad (9)$$

so the first derivative  $dh/dt$  amplifies the noise contained in  $h$  as a function of frequency  $f$ , the Fourier transform of the second derivative  $d^2h/dt^2$  is directly proportional to frequency squared. The general expression given by Eq. (9) does not apply exactly to the polynomial smoothing filters, described in the previous

subsection; the major part of the noise component is indeed strongly amplified, however, the filter also smoothes the highest-frequency part of the signal; at low frequencies, there is also a deviation caused by the fact that the functions under consideration are defined in a limited (non infinite) time interval.

We used the presented inversion method first to calibrate the GRACE onboard accelerometers (Bezděk, 2010). We showed that in the along-track direction the variations in acceleration due to nongravitational perturbations are approximately of the same order of magnitude as the variations from the gravity field terms of degree 50. In this case, the simulated 1-cm white noise  $\varepsilon^*$  in GPS positions is amplified by taking  $\varepsilon=d^2Q(\varepsilon^*)/dt^2$  to be at least 100 times larger than the studied gravity signal  $\mathbf{a}_{\text{grav}}$  (ibid, cf. Figs. 1 and 5, where the signal is around  $10^{-7} \text{ m s}^{-2}$ , while the noise  $10^{-4} \text{ m s}^{-2}$ ). Stated otherwise, the cited figures in Bezděk (2010) show that due to the action of the second-derivative filter, the noise in GPS positions was indeed amplified at least 100 times for gravitational accelerations of interest. (Since atmospheric drag has varied considerably during the GRACE lifetime, we note that these results apply to GRACE orbital data from the year 2003. Degree 50 was found by computing acceleration induced by the individual terms of the geopotential spherical harmonic series and by comparing the magnitude of these accelerations to that of the nongravitational accelerations in the along-track direction (ibid, p. 413).)

*Problem of autocorrelated errors* — The Gauss-Markov theorem states that in a linear model in which the errors have expectation zero, are uncorrelated and have equal variances, the best linear unbiased estimator of the coefficients is given by the ordinary least-squares (OLS). Here ‘best’ means that the OLS estimator has the smallest variance (e.g. Brockwell and Davis, 2002, p. 385). Observations gathered from experimental time series tend to have errors that are correlated since they are affected by similar external conditions. The presence of autocorrelation can be a problem of serious concern for the following reasons: (i) The OLS estimators continue to be unbiased, but are no longer the best estimators. (ii) The errors in the regression coefficients may be seriously underestimated. Thus, the confidence intervals and various tests of significance commonly employed would no longer be strictly valid (Chatterjee and Hadi, 2006; Rawlings et al., 1998).

When a digital filter is applied to a signal containing a random component, the random errors residing at each data point within the filter window are linearly combined to the new output value; thus the newly formed vector has a random component, which is autocorrelated. This is what happens when the polynomial derivative filter  $F$  is applied to the time series  $\mathbf{r}_{\text{gps}}$  of GPS positions. As mentioned, the studied geopotential signal  $\mathbf{a}_{\text{grav}}$  is much smaller compared to the noise component  $\varepsilon$ . In our experience, the correct fit of the geopotential coefficients becomes complicated even for the idealized simulated data with correlated errors, because the noise correlation structure may create long-wave artefact pseudo-signals, which may bias the OLS estimates.

Let us rewrite our regression model (7) in the usual statistical notation

$$y = Xb + \varepsilon, \quad (10)$$

where the vector of observations is  $y=d^2Q(\mathbf{r}_{\text{gps}})/dt^2 - \mathbf{a}_{\text{other}}$ , the design matrix  $X=[\nabla V_{nm}^{(c)}; \nabla V_{nm}^{(s)}]$  and the vector of estimated parameters  $b=[C_{nm}; S_{nm}]$ . Suppose that from post-fit residual analysis and tests we have reason to believe that the error covariance matrix is not equal to a scaled identity matrix,  $\text{Var}(\varepsilon) \equiv \sigma^2 V \neq \sigma^2 I$ . The *generalized least squares* (GLS) then define a linear transformation

$$W = T^{-1}, \quad \text{where} \quad V = TT', \quad (11)$$

which maps the original linear model into a new one,

$$y^* = X^*b + \varepsilon^*, \quad (12)$$

such that the covariance matrix of the transformed errors  $\varepsilon^*$  becomes again a scaled identity matrix (e.g. Brockwell and Davis, 2002; Rawlings et al., 1998). Indeed,

$$\text{Var}(\varepsilon^*) = W\text{Var}(\varepsilon)W' = \sigma^2 T^{-1}TT'T^{-1'} = \sigma^2 I. \quad (13)$$

In the transformed variables,  $y^*=Wy$ ,  $X^*=WX$ , and the usual OLS are then used to find the regression parameters  $b$  of the *original* problem with correct estimates of their uncertainties. A simple numerical example comparing the OLS vs. GLS estimates is in Bezděk (2010, App. B).

In fact, the non-diagonal covariance matrix of the acceleration random component  $\varepsilon$  in Eqs. (7) and (10) was created by the action of the second-derivative filter  $F$ . Suppose now that the noise in GPS positions is white, so its covariance matrix is  $\text{Var}(\varepsilon^*)=\sigma^2 I$ . Then,

$$\text{Var}(\varepsilon) = \mathbb{F}\text{Var}(\varepsilon^*)\mathbb{F}' = \sigma^2 \mathbb{F}\mathbb{F}', \quad (14)$$

where  $\mathbb{F}$  is a square matrix, generated from the coefficients of the polynomial filter  $F$  and whose multiplication is equivalent to the action of the filter (e.g., Gray, 2006). But the situation, where we *know* the covariance matrix of the random errors in a linear model, is exactly what the GLS method is suited for. In our case, finding the GLS transformation matrix is straightforward,

$$\mathscr{W} = \mathbb{F}^{-1}. \quad (15)$$

After applying  $\mathscr{W}$  to the linear model (10) and after solving the transformed equation (12) through the OLS, the residuals are again uncorrelated and the original  $\sigma^2$  may be estimated.

Eq. (15) points out the meaning of the GLS transformation matrix in that it transforms the model originally formulated in accelerations back to positions. As for the actual implementation, we compute the matrix  $W$  from Eq. (14); first, the lower triangular matrix  $T$  is found through the Cholesky decomposition of the covariance matrix  $\mathbb{F}\mathbb{F}'$ , then we obtain the matrix  $W$  from  $T$  by its inversion (Eq. 11). The thus computed matrix  $W$  is not equal to  $\mathbb{F}^{-1}$ , but this is not a problem, in fact we only need Eq. (11) to be fulfilled. The first and last few numerical derivative vectors  $d^2Q(\mathbf{r}_{\text{gps}})/dt^2$  are not valid as an approximation to the observed acceleration vectors  $d^2\mathbf{r}/dt^2$  because of the filter transition phase. Therefore, we discard the corresponding few first and last lines from the regression system (10), and also from the filter matrix  $\mathbb{F}$ , which is on the input to the Cholesky decomposition.

Summarizing the contents of this subsection, application of a numerical double differentiation filter to GPS positions in order to obtain an approximate acceleration vector is possible, but

has drawbacks in that the noise in GPS positions is strongly amplified and becomes autocorrelated. Both of these problems are solved by a linear transformation of the regression model (7). The transformation matrix  $W$  is found through the application of the GLS estimation method. Correct estimates of the model parameters and their uncertainties are found from the transformed model using OLS.

#### 2.4. Decorrelation of errors in GPS positions

The GLS transformation matrix  $W$  defined in Eq. (15) is a sort of inverse mapping to get from the acceleration domain back to the position domain. As a test of the transformed regression model (12), using a known geopotential model (e.g. EIGEN-6S, Förste et al., 2012) we can generate precise satellite positions, which will represent the ‘true orbit’, and add to them 1-cm uncorrelated normally distributed errors. This ‘true’ orbit with added noise represents the input positions  $r_{\text{gps}}$  to our observation equations (7), from which the satellite accelerations are obtained as described in Sect. 2.2 and the system of observation equations is decorrelated according to Sect. 2.3. The solution of the GLS-transformed linear system (12) produces the original harmonic coefficients, and the regression residuals are indeed uncorrelated normally distributed with an estimated standard error close to 1 cm.

At this point, the real-world GPS positions of low Earth satellites enter the method development. If instead of the simulated orbits with idealized white noise, real GPS positions are used to obtain the geopotential harmonic coefficients, systematically the regression residuals are strongly correlated. In the left panel of Fig. 2, the sample autocorrelation function (ACF) displays strong correlation of the residuals obtained by solving the transformed linear system (12).

The fact that the random errors in the neighbouring GPS positions are correlated is not surprising (Baur et al., 2012; Ditmar et al., 2007; Jäggi et al., 2011c; Reubelt et al., 2003). During a small time step between two consecutive GPS observations of a low-Earth satellite (e.g. 10 seconds for CHAMP), the constellation of the much higher flying GPS satellites used to determine the two positions is almost the same. In Fig. 2, the estimated correlation length is about 25 min (a lag of 50), i.e. about a quarter of the orbital period of GRACE B.

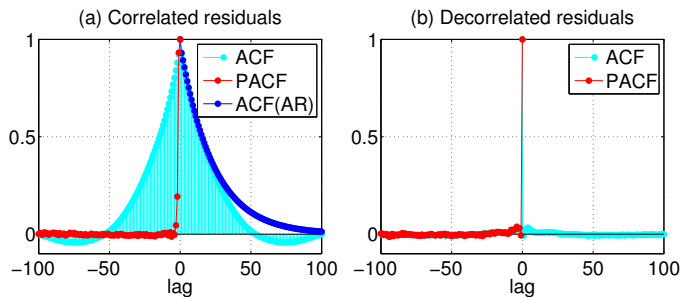


Figure 2: Sample statistics of the fit residuals; on the left, residuals from the once-transformed model (12), on the right, residuals from the twice-transformed model (16). Symbols: ACF sample autocorrelation function, PACF sample partial autocorrelation function, ACF(AR) autocorrelation function for the fitted AR model, for details please see the text. Data: GPS positions of GRACE B spanning the year 2009, the unit of lag (time interval) is 30 sec.

*Autoregressive model* — In time series analysis, after deterministic components like trends and seasonal variations have been removed, in order to use statistical inference we may try to represent the behaviour of the stationary residuals by some simple probabilistic model. Apart from the moving average model, which was already mentioned when speaking about the differentiation filter, another useful class of time series models are the autoregressive processes. Loosely speaking, a sequence of independent random variables  $Z_t$  as a function of time  $t$  may be transformed into a new output sequence by two basic ways. We can define a running window of a finite length and combine the input values  $Z_t$  within the window to produce a new output random variable  $X_t = \sum_k \theta_k Z_{t-k}$ , where  $\theta_k$  are constant weighting factors. Another possibility to create a correlation structure is to use recursion, the output value  $Y_t$  at time  $t$  is given as a linear combination of the preceding output values,  $Y_t = \sum_{k=1}^p \phi_k Y_{t-k} + Z_t$ , where  $\phi_k$  are model parameters. In this way an *autoregressive model of order  $p$* ,  $AR(p)$ , is defined.

In the same way as the autocorrelation function is used to identify the correlation length for moving average models, the order of an autoregressive model may be estimated from the sample *partial autocorrelation function* (PACF). For an  $AR(p)$  process the partial autocorrelation function is zero for lags greater than  $p$ . In practice, if an  $AR(p)$  model is appropriate for the data, then the values of the sample PACF for lags greater than  $p$  should be compatible with observations from normal distribution  $N(0, 1/n)$  with zero mean and standard deviation  $\sigma^2 = 1/n$ , where  $n$  is the number of samples. For a more detailed explanation of time series analysis methods see e.g. Brockwell and Davis (2002). We note that usage of autoregressive models in the context of satellite gravity gradiometry was recently discussed several times, see e.g. Schuh (1996); Klees et al. (2003); Siemes (2008).

*Fitted AR model and decorrelation of residuals* — In the left panel of Fig. 2, the sample PACF, computed from the residuals of the model (12), falls rapidly towards zero at lags higher than 4, which is an indication that an  $AR(4)$  model may be a suitable representation of the correlation structure in the GPS positions. We estimated the AR model parameters through Yule-Walker equations (Brockwell and Davis, 2002, p. 139). The autocorrelation function of the fitted model,  $ACF(AR)$ , now approximates the original ACF. Again we have a linear system with autocorrelated errors, as in the previous subsection, but now the correlation originates from the nature of the closely spaced GPS positions. To decorrelate the residuals, we may apply the GLS method once more. In accordance with its definition (11), the GLS transformation matrix  $W^*$  may be found by the Cholesky decomposition of the covariance matrix of the fitted AR model. The whole decorrelation procedure can easily be made automated. We allow the maximum lag of the fitted PACF to be 100 and this is also the limit for the automatically estimated order  $p$  of the fitted  $AR(p)$  model. For later reference, by double asterisk we will denote the twice-transformed linear model

$$y^{**} = X^{**}b + \epsilon^{**}, \quad (16)$$

which was obtained from the once-transformed model (12) by applying the linear transformation matrix  $W^*$ . Finally, the right panel of Fig. 2 shows that the residuals of the twice-transformed model (16) are indeed approximately uncorrelated. In the rest of the paper, when we speak about ‘decorrelated’ quantities, e.g. decorrelated residuals or decorrelated solutions, we mean that they were obtained from the twice-transformed model (16).

In Fig. 3 we show a comparison of the yearly GRACE B solution with correlated residuals (in blue) and the solution with decorrelated residuals (in red). Systematically, our results show that the decorrelation based on the fitted AR model not only improves the estimated error bars, and makes them more realistic, but there is an appreciable improvement in the estimated harmonic coefficients as well. The coefficients from the decorrelated model (16) are more accurate by a factor of 2–3 for degrees higher than 20; there is a smaller but still visible improvement for lower degrees.

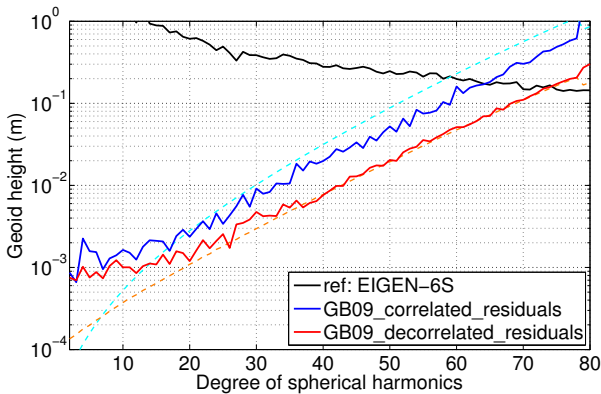


Figure 3: Degree difference amplitudes between estimated and reference harmonic coefficients. Decorrelating the errors in GPS positions improved the solution by a factor of 2–3. Also errors of estimated parameters (dashed lines) are now more realistic. Data: GRACE B, year 2009.

In order to represent the correlation structure found in the error component of the observed GPS positions, we introduced a fitted autoregressive process, whose order was estimated by using the sample partial autocorrelation function. In accordance to Brockwell and Davis (2002, Ch. 1), we applied a general approach to time series analysis of this correlation structure. After removing deterministic components to produce a stationary series of residuals, we looked for a hypothetical probability model to represent the data, making use of various sample statistics including the sample ACF and PACF. Then, an appropriately chosen model compatible with the data may be used in a variety of ways depending on the particular field of application, in our case for decorrelating the residual time series so that we can draw correct statistical conclusions regarding the estimated coefficients. The motivation for using the sample PACF lies in its ability to simply identify the order of the underlying AR process. As one is used to speak about a correlation length, which is easily found by looking at the graph of sample ACF, in exactly the same way, a quick visual inspection of the graph of sample PACF yields an estimate of the order of an AR process. Figure 2(a) shows that the ACF of an AR process decays exponentially compared to a much simpler graph of the sample PACF, which rather quickly

goes to zero. The appropriateness of using the fitted AR process to represent the correlations in GPS errors is demonstrated by the fact that after decorrelating the residuals, not only the error bars become more realistic, but also the fitted geopotential coefficients visibly improved.

## 2.5. Other implementation details

Our inversion method is implemented in Matlab (<http://www.mathworks.com/>). All the computations were done on an ordinary PC up to harmonic degree 120. For the calculation of the partial derivatives matrix  $X$  we first used the modified forward row method (Holmes and Featherstone, 2002), currently we use a faster algorithm based on Hotine’s equations (Sebera et al., 2013). A further speed up of the partial derivatives computation is achieved by writing this function in the C language and compiling it as the Matlab MEX-file.

As already emphasized, after two linear transformations of the regression model (10), we assume that the errors are approximately independent normally distributed and ordinary least squares are used to solve the twice-transformed system (16). Due to the huge number of observations, the system of normal equations has to be built up sequentially (Weigelt, 2007). For each studied mission we tested using data blocks of variable size; the obtained results were different for different number of observations comprised in a block. The block size depends on the maximum harmonic degree of the solution sought and is limited by the available amount of the RAM memory (24 GB in our case). The longer block size, the shorter computation time, but sometimes also worse results for longer blocks were obtained. So far, we found the optimum block size for the 10-sec CHAMP orbits to be approximately a half of the orbit period and two orbital periods for the 30-sec GRACE A/B orbits. Preliminary block size for the 1-sec GOCE orbits is a tenth of an orbital period. Similarly to the parameters of the differentiation filter (Sect. 2.2), the block size turned out to be an important defining parameter of our inversion method having direct influence on the accuracy of the computed solutions.

One can ask why the data block size may have an influence on the results of the inversion. If we had a linear regression problem, then cumulating the normal matrix using blocks would produce exactly the same solution, for any block length. However, this ideal situation is disturbed by the application of the linear transformation matrix. In principle, the order of this square matrix should equal the number of rows of the design matrix; the transformation is to be applied to both sides of the linear system. Unfortunately, the number of rows (number of observation points in the processed time period) is too large for the design matrix to enter the RAM memory. For example, for a month of 10-sec positions, for a field of maximum degree 100, for three components, we would need some 62 GB of the RAM memory. Furthermore, GOCE and the forthcoming Swarm satellites have 1-sec orbits. This is the reason for the necessity of cumulating the normal matrices by blocks, and thus introducing an error by putting some parts of the transformation matrix equal to zero (i.e. those parts of ideal large transformation matrix, which are outside the data block processed; this error is somewhat reduced by the fact that the elements of the transformation matrix  $W$  above the main diagonal are already equal to zero).

On the other hand, if the noise happens to be nonstationary, then longer blocks may cause problems (Pavel Ditmar, priv. comm.). The longer the block, the wider the frequency range under consideration. Since the frequency-dependent data weighting is applied that compensates the effect of double differentiation (which amplifies noise proportionally to the frequency squared), the weights assigned to low frequencies may become large, as compared to weights assigned to high frequencies. This observation may explain the fact that we found different values of optimum block lengths for CHAMP and GRACE orbits (together with different sampling time).

As already mentioned, we use the nongravitational accelerations measured by the onboard accelerometers. Previous experience showed that the calibration of onboard accelerometer readouts was rather complicated, due to a very high correlation between the accelerometer biases and scale factors (Bezděk, 2010). Therefore, we first fitted the accelerometer readouts to the simulated nongravitational signal, and then we used such calibrated accelerometer observations  $a_{NG}$  in the regression model (7). The simulated nongravitational accelerations comprised drag, direct solar radiation, albedo effect and Earth infrared radiation (for details, please see Sect. 2.2 of Bezděk, 2010). To have a realistic drag coefficient, for each satellite we estimated its value using long-term change in orbital elements (months to years). To obtain cross-sectional area in the direction of motion, we used satellite macro-models. In case of CHAMP accelerometer data, due to a hardware error we replaced the observations in the accelerometer radial component with simulated nongravitational accelerations. When accelerometer observations were used, we expressed the linear model (7) in the accelerometer-fixed reference frame that is up to a few degrees close to the satellite local reference frame, which was used otherwise (Sect. 3.2). This discussion applies to accelerometer observations of CHAMP and GRACE A/B satellites, in computing preliminary results pertaining to GOCE we made use of simulated nongravitational accelerations. Based on the shape, dimensions and mass of the GOCE satellite, we assess the nongravitational accelerations in the cross-track and radial directions, we assume that the along-track component is negligible due to the drag-free control system. We tested the validity of this approach by using real GOCE accelerometer data.

For processing the satellite orbital data, coordinate transformations and generation of simulated data, we used our own orbital propagator NUMINTSAT (Bezděk et al., 2009). For the final version of this paper, we used: transformations between ICRS and ITRS systems according to IERS Conventions 2010 (Petit et al., 2010), lunar and solar ephemerides JPL DE405 (<ftp://ssd.jpl.nasa.gov/pub/>), model of solid Earth tides (anelastic Earth; McCarthy, 1996), model of ocean tides FES 2004 (Lyard et al., 2006), model of relativistic correction (McCarthy, 1996), model of neutral thermospheric density DTM-2000 (Brunisma et al., 2003). We used the kinematic orbits of CHAMP and GRACE satellites given in IGS05 geodetic datum (Prange, 2010). As stated earlier, our solutions obtained by the inversion of GPS positions of real satellites do not need any a priori gravity field models; for generating simulated data and performing other tests, we made use of various gravity field models, e.g. EGM2008 (Pavlis et al., 2012), GGM03 (Tapley et al., 2007),

ITG-Grace2010s or EIGEN-6S. In processing the orbits of the satellites CHAMP, GRACE A, GRACE B and GOCE, our gravity field models presented in Sect. 3 were produced from the considered data sets individually, not jointly. This applies also to the treatment of time-variable gravity field in Sect. 3.9, the individual solutions are each time based only on the data of the satellite mission in question. We note that for correct estimates of the coefficients  $C_{21}$ ,  $S_{21}$ , a contribution of the solid Earth pole tide (Petit et al., 2010, p. 93) proved to be substantial.

Every point of CHAMP and GRACE A/B kinematic positions (Sect. 3) was accompanied with an uncertainty estimate (formal errors included in the orbit products). In some cases, e.g. with CHAMP orbits in the years 2006 and 2009 when its onboard GPS receiver had hardware problems, using the estimated uncertainties somewhat improved the solution, in other cases, e.g. with CHAMP positions in 2008, the solutions did not appear to be better. We think that this is due to the application of the decorrelation procedure (Sect. 2.4), which has a considerable effect on the random component of GPS positions.

By their construction kinematic positions contain outliers and data screening is a necessary processing step (e.g. Prange, 2010). Excluding outliers is indeed important to obtain meaningful geopotential solutions; we do this by repeatedly fitting the solution and by excluding gross outliers using the four-sigma criterion. This criterion is applied to the residuals of the twice-transformed model (16).

The number of other estimated parameters is very small, apart from the geopotential coefficients we only included daily biases (i.e., a constant term added to Eq. 7).

In Sect. 2.2 we mentioned that during the method development a use was made of noise with different characteristics. Based on the analysis of the observation residuals computed using the real GPS positions (Sect. 2.4), apart from using the white noise, in the simulations we also modelled the noise as realizations of the low-order AR processes (e.g. the one, whose ACF is shown in Fig. 2).

### 3. Results

In the preceding section, the main components of our inversion procedure were described. We formulated the regression model (7) which is linear in the unknown geopotential harmonic coefficients. Problems of high-frequency noise amplification and of autocorrelated errors in GPS positions were resolved by two linear transformations of the initial regression system (10), so that the residuals finally became approximately uncorrelated normally distributed. In accordance with the generalized least squares method (Sect. 2.3), the ordinary least squares may be applied to the twice-transformed regression model (16). By solving the normal equations we obtain estimates of the harmonic coefficients accompanied by their full covariance matrix.

*Kinematic orbits* — In the classical inversion methods, observation equations are linearized with respect to the fitted parameters and for estimating the geopotential coefficients an a priori gravity field model is needed (e.g. Montenbruck and Gill, 2000, Ch. 7–8). In this way, the geopotential coefficients are

obtained by adding corrections to their a priori values, and the resulting geopotential model may be somewhat biased towards the a priori field. Also the GPS-SST positions themselves may be influenced by force models involved in dynamic or reduced-dynamic orbit determination. This is the reason why in the acceleration approach it is advisable to derive accelerations from kinematic orbits, where the position points are determined purely geometrically from GPS measurements without any information about forces that influence the satellite motion (Ditmar et al., 2006; Sluijs, 2002; Reubelt et al., 2003, 2006; Švehla and Rothacher, 2005). (We note here that a priori gravity field information is implicitly used through the GPS ephemeris, but this will have a minor impact due to the high altitude of the GPS satellites and their global distribution.) In our computations we used the kinematic orbits of CHAMP and GRACE A/B satellites from AIUB (Jäggi et al., 2009, 2011b), and the kinematic orbits of GOCE, which are one of the Level-2 products (EGG-C, 2010; Bock et al., 2011).

### 3.1. Gravity field from one day of real data

There is a dramatic difference between the global (satellite) gravity field models from the era before CHAMP, and with CHAMP, GRACE and GOCE. The older models not only had less precise data (electronic, photographic, a first generation laser), but also were not continuous in time and space like the GPS high-low SST data available now. The inversion from the old observations to the gravity field coefficients required data gathered from many satellites and long observation times to ensure the stability of the inversion. Moreover, the functional models were solely nonlinear, which added to the complexity of the inversion (e.g., reasonable starting values for the fitted geopotential coefficients). Today, we can create a test long-wavelength gravity field model with CHAMP or GRACE or GOCE from observations covering one day.

In Fig. 4, for the three missions studied we show the results of an inversion of GPS positions, which were acquired during only one day. From these precise GPS positions observed at constant time step of 1, 10 or 30 seconds, we obtained decent gravity field models complete to degree and order 15. By this example we emphasize the novelty of the GPS-SST observational data type. To compute the daily gravity field models shown in Fig. 4, we used the *linear* regression model (7) and solved it using the ordinary least squares. The tiny orbital perturbations caused by higher degree and order terms of the Earth gravity field are sufficient to yield all the sought 255 geopotential coefficients in one step and without any a priori gravity field model. Only Newton's law, models of other perturbing forces (Eq. 6) and 3D orbital points measured accurately and densely enough in space and time are needed and used.

In addition, the bottom two panels of Fig. 4 show the corresponding daily ground track; they will be very helpful in the next subsection. Presently there is a discussion about the theoretical and practical limit on what maximum degree and maximum order solution may be obtained from such near polar circular orbits (e.g. Weigelt et al., 2013b; Klokočník et al., 2008).

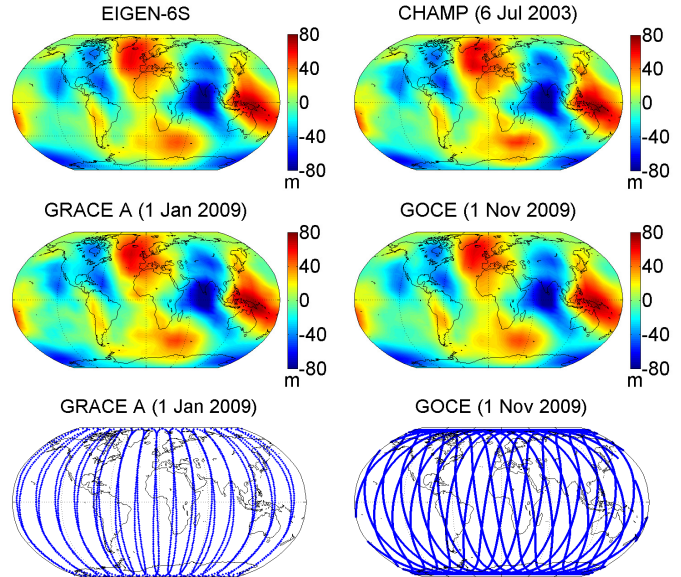


Figure 4: Map of geoid heights computed from EIGEN-6S model (as a reference), then similar maps of our daily solutions, all computed to maximum degree 15. Bottom panels: the corresponding ground tracks for the orbits used in our one-day inversions. (Ground tracks of CHAMP are not shown, they are similar to those of GRACE A.)

### 3.2. Combination of along-track, cross-track and radial solutions

*Satellite local reference frame* — Linear regression model (7) is a pointwise vector equation, therefore it is possible to project it into a suitable reference frame. It is well known that GPS positions have different uncertainty in the horizontal and vertical directions (e.g. Hofmann-Wellenhof et al., 2008). Taking into account that all the satellites in question are attitude stabilized with respect to their velocity vector and Earth (to within a few degrees), after having done the differentiation in the inertial reference frame, we transform the regression model to the satellite local reference frame (LRF). The three LRF components are defined as along-track (A-T; projected to the velocity direction), cross-track (C-T; direction of angular momentum) and radial (RAD; almost radial, it completes the right-handed system).

*Combination solution using normal matrices* — In the rest of the paper we will speak about OLS solutions of the twice-transformed model (16), but we drop the double asterisk. Assuming that the error covariance matrix is a scaled identity matrix,  $\text{Cov}(\varepsilon) = \sigma^2 I$ , the solution vector  $\hat{b}$  and its covariance matrix  $\text{Cov}(\hat{b})$  may be written

$$\hat{b} = N^{-1} X^T y, \quad \text{Cov}(\hat{b}) = \hat{\sigma}^2 N^{-1}, \quad (17)$$

$$N = X^T X, \quad \hat{\sigma}^2 = \frac{(y - \hat{y})^T (y - \hat{y})}{r - s}, \quad (18)$$

where  $N$  is the normal matrix,  $\hat{\sigma}^2$  estimated error variance,  $r$  number of observations,  $s$  number of estimated parameters. We obtain three solution sets (17), (18), one for each LRF component; supposing they are independent, the combined solution  $\hat{b}_c$  is given by

$$\hat{b}_c = \sum_i R_i \hat{b}_i, \quad \text{Cov}(\hat{b}_c) = N_c^{-1}, \quad (19)$$

$$R_i = N_c^{-1} \hat{\sigma}_i^{-2} N_i, \quad N_c = \sum_i \hat{\sigma}_i^{-2} N_i, \quad (20)$$

where the index  $i=\{\text{'a-t'}, \text{'c-t'}, \text{'rad'}\}$  denotes the individual LRF components. Unless stated otherwise, all the presented satellite solutions are the combined ones (19). As regards the assumption about the independence of the individual LRF component solutions, we suppose that the sensitivity to geopotential harmonic coefficients is different for each LRF direction, and as such these directions provide complementary information.

*Contribution graphs* — In a direct analogy to the weighted mean, where each contributing point is weighted by its inverse variance normalized by the sum of the inverse variances, the weighting factors  $R_i$  in the combined solution (19) are matrix versions of the normalized inverse variances. If these matrices  $R_i$  are diagonally dominant, which is generally the case for our solutions (Sect. 3.7), then visualizing elements on their main diagonal has an interesting and informative interpretation (cf. Yi and Rummel, 2011). The  $k^{\text{th}}$  diagonal element of  $R_i$  is the relative weight with which the  $k^{\text{th}}$  component of the individual solution vector  $\hat{b}_i$  contributes to the  $k^{\text{th}}$  component of the combined solution  $\hat{b}_c$ .

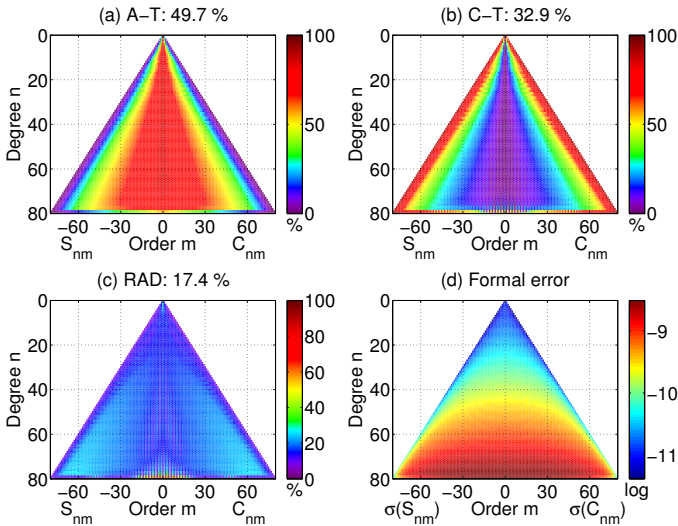


Figure 5: Contribution graphs for the individual LRF solutions. Bottom right panel: standard errors of the combined solution. Data: GRACE B, 2009.

In Fig. 5 these relative contributions are depicted in percentage terms for a yearly GRACE B solution. In the upper left panel, relative contribution of the along-track solution is maximal for the zonal and near-zonal harmonic coefficients. This can easily be understood by looking at the satellite ground tracks in Fig. 4. For polar orbits, the A-T direction is oriented north-south, where most signal energy from zonal harmonics is located. On the other hand, the cross-track component is directed east-west relative to Earth, thus the C-T component is most sensitive and contributes the most to the sectorial harmonics, as is shown in the upper right panel of Fig. 5. In the title of the contribution graphs also the mean relative contribution of each component is given. The quoted percentages are typical for our solutions, on average the A-T solution contributes by 35–50 %, the C-T by 30–45 %, the RAD by 15–20 %. The formal standard errors of the obtained

harmonic coefficients are in the lower right panel of Fig. 5.

As mentioned, all the presented solutions were acquired by combining the separate LRF solutions (if not stated otherwise). We also tried to solve the regression model in other reference frames (celestial, Earth-fixed), but systematically the best results were obtained with Newton’s law expressed in LRF. A possible explanation of this fact might be the following. Each of the three individual LRF solutions has not only its own formal covariance matrix  $N_i^{-1}$ , but also its own standard error of the fit  $\hat{\sigma}_i$ . Systematically these errors are different for the three LRF solutions, thus every solution  $\hat{b}_i$  enters the combined solution  $\hat{b}_c$  weighted *individually* by its corresponding factor  $R_i$ , Eqs. (19)–(20). Also the information contained in the individual LRF solutions, as graphed in Fig. 5, is different and complementary. When we solved the regression system (7) in the celestial reference frame, the individual sigmas  $\hat{\sigma}_i$  of the three solutions in the corresponding Cartesian components were similar to each other, as well as the mean contribution of the three solutions. We see the explanation of why the LRF provides better solutions in the fact that the LRF is better suited for modelling the properties of the random component in the observed GPS positions (cf. Baur et al., 2012).

### 3.3. Along-track solution vs. combined solution

A widely used method of estimating the geopotential coefficients from GPS kinematic positions is the so-called energy balance approach (e.g. Földvary et al., 2005; Sneeuw et al., 2005; Weigelt et al., 2009). There the information from GPS positions is projected solely to the satellite velocity direction; compared to the three-dimensional character of the acceleration approach or the celestial mechanics approach (Beutler et al., 2010a,b), methods based on energy balance are expected to produce geopotential solutions worse by a factor of  $\sqrt{3}$  (Baur et al., 2012; Ditmar and Sluijs, 2004).

In our method, we can easily compare the individual A-T only solution with the combined solution. It is clear from the contribution graphs in Fig. 5 that the combined solution benefits substantially from all the three LRF solutions. In Fig. 6 the factor with which the yearly combined solution outperforms the A-T solution varies between 1.2–2.0, comprising the quoted value of  $\sqrt{3}$ . Even if our A-T solution is not equivalent to an energy balance solution, this result confirms that it is advantageous to exploit the 3-D orbital information compared to its 1-D projection.

Due to the GOCE orbital inclination, polar gaps arise with an angle of  $6.7^\circ$ , which are uncovered by satellite ground tracks and which bring about problems in the determination of the near zonal harmonic coefficients (e.g. Baur et al., 2012; Sneeuw and van Gelderen, 1997). In Fig. 7 we show that for the GOCE solution to degree 75 indeed the A-T only solution exhibits considerably worse near-zonal coefficients (left panel), but in the combined solution this unwanted effect is significantly reduced (right panel). This polar gap problem is negligible in the GRACE and CHAMP solutions, because their orbits are close enough to the poles.

### 3.4. Degree difference amplitudes

In Figs. 6 and 7, to show the quality of our GPS-SST solutions we used their difference with respect to geopotential models

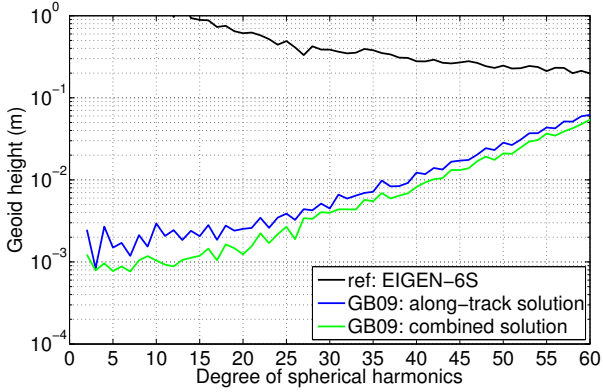


Figure 6: Degree difference amplitudes of the estimated harmonic coefficients related to reference field. Data: GRACE B, 2009.

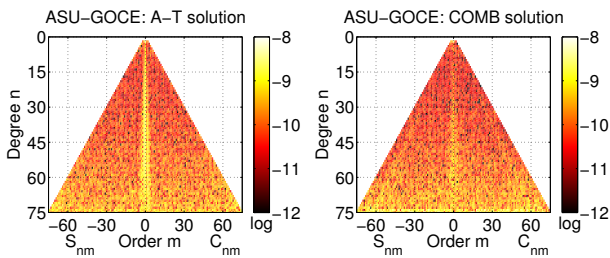


Figure 7: Two-dimensional difference spectrum between estimated harmonic coefficients and EGM2008 model. Data: GOCE, Nov–Dec 2009.

containing a contribution from GRACE KBR data (e.g. EIGEN-6S, EGM2008). As mentioned in the introduction, currently the GRACE KBR based gravity fields are the best static geopotential models available for harmonic degrees up to 100–150 (Pail et al., 2011b). Thus, we assume that individual GRACE KBR geopotential coefficients up to degree and order 100 are more accurate with a factor of 10–100 compared to those from our GPS-SST solutions. This is the reason for the capability of GRACE KBR solutions to be used in the sense of a measurement standard (etalon), as a ‘truth’, for assessing the quality of the GPS-SST geopotential solutions. *Degree difference amplitudes*, used in figures throughout this paper, enable comparison of two geopotential models as a function of degree  $n$  (Prange, 2010) and are defined as

$$DDA_n = R \sqrt{\sum_{m=0}^n (\Delta C_{nm}^2 + \Delta S_{nm}^2)}, \quad (21)$$

where  $\Delta C_{nm}$ ,  $\Delta S_{nm}$  are the differences in the coefficients of the two models (cf. Wagner and McAdoo, 2012). In analogy to spherical approximation used in physical geodesy, we added the Earth radius  $R$  to the definition of degree difference amplitudes to express them in terms of geoid height (and thus in metres). For a given GPS-SST model and various reference fields, the degree difference amplitudes are virtually the same, provided the longwave part of the reference model is based on GRACE KBR data. As a reference model we preferred to use EIGEN-6S, because for the lowest degree coefficients this model provides time variations for the period studied, which are not negligible in the difference graphs. Our multi-year solutions combine in-

formation from all the yearly solutions included, so in the degree difference amplitudes we used the time-dependent values of EIGEN-6S at the mid-epoch of the multi-year solution (e.g. 2006.5 for our CHAMP or GRACE 2003–2009 solutions). To compute the EIGEN-6S harmonic coefficients for use in degree difference amplitude graphs, we used the full time-related information (mean, trend, annual variation) as given in the model data file.

### 3.5. Gravity field model from orbit of CHAMP in 2003

As mentioned in the introduction, with very long time series of precise GPS positions, accompanied by onboard accelerometer measurements, CHAMP opened a new era in gravity field modelling, not only because of higher accuracy of new global geopotential models, but also as a stimulus for developing new computational methods. This is also the reason why the ‘Table of models’ of the ICGEM website provides quite a number of solutions based on CHAMP data spanning the first years of the mission. Fig. 8 shows some of these models. TUM-2S is an energy balance solution based on two years (2002–2004) of CHAMP GPS and accelerometer data (Wermuth et al., 2004); AIUB-CHAMP01S is a one-year gravity field model (2002–2003) using the celestial mechanics approach (Prange et al., 2009); ITG\_Champ01S is a one year solution (03/2002–03/2003) based on the formulation of Newton’s equation as a boundary value problem (Mayer-Gürer et al., 2005); EIGEN-CHAMP03S is a CHAMP-only gravity field model derived from GPS and accelerometer data covering 2.8 years (2000–2003) with regularization starting at degree 60 (Reigber et al., 2005a). The regularization is the cause for the EIGEN-CHAMP03S curve to ‘follow’ the signal of the reference model beyond degree 60. The very satisfactory behaviour of our yearly solution ASU-CHAMP-03 is certainly due to the excellent kinematic orbits computed at AIUB, whose quality has been steadily improving (Jäggi et al., 2009; Bock et al., 2011; Prange et al., 2010). We used the CHAMP kinematic orbits spanning the year 2003. As already mentioned, we do not use any regularization scheme in our solutions. (We note here that truncating the gravity field estimation at a certain maximum degree is also a sort of regularization.)

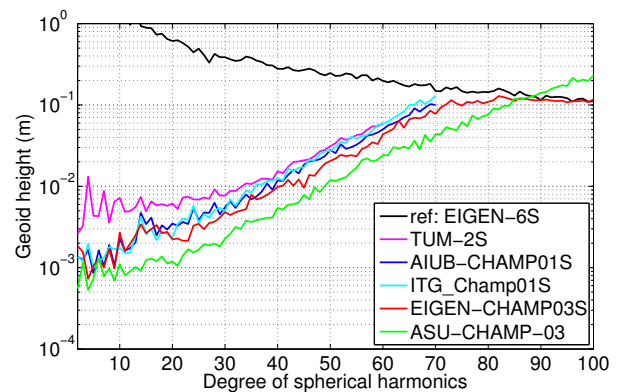


Figure 8: Degree difference amplitudes of several geopotential models related to reference field. Data: CHAMP, 2000–2003, period different for the individual models.

### 3.6. Seven-year solutions from CHAMP and GRACE orbits

By Eqs. (19) and (20) we defined the combination of individual LRF solutions using the weighting matrices  $R_i$ . In the same way we can combine the yearly solutions of CHAMP and GRACE A/B satellites to obtain yearly mean seven-year geopotential models separately for each satellite, which are shown in Fig. 9. For degrees greater than 20, better accuracy of the long-term static CHAMP solution is caused by the lower altitude of CHAMP satellite (300–420 km) compared to that of GRACE A/B satellites (440–500 km) over the studied period. Both the GRACE solutions are of similar accuracy over all harmonic degrees.

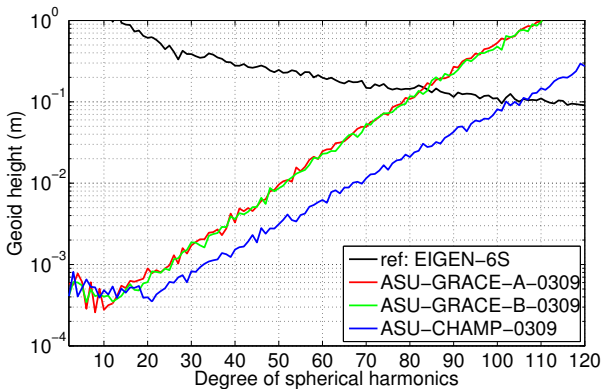


Figure 9: Degree difference amplitudes of our seven-year static gravity field models related to reference field. Data: GPS-SST, 2003–2009.

In Table 1 we give relative contributions of individual yearly solutions into their seven-year combined solutions. Considering the attenuation with altitude of higher degree spherical harmonic terms proportional to  $r^{-n}$  in Eq. (1), one may expect that on average the last years of each mission would contribute more to the combined solution, because of the gradually decreasing satellite altitude. This is the case for the GRACE A/B satellites, however there are apparently other factors which modify this general rule. As for CHAMP, since October 2008 due to serious onboard hardware problems the accuracy of its GPS positioning became considerably reduced (Prange, 2010), but owing to the satellite’s low altitude the average contribution of the 2009 CHAMP solution to the combined seven-year model is relatively high.

Table 1: Average relative contribution of yearly solutions into the respective combined 7-year solution for each satellite (percentage).

Year	CHAMP	GRACE A	GRACE B
2003	6.3	10.8	12.9
2004	7.1	12.8	13.7
2005	16.0	10.2	6.2
2006	16.0	12.3	11.5
2007	18.2	16.1	18.6
2008	21.5	18.7	16.7
2009	14.9	19.1	20.4

In Fig. 10 we compare our long-term CHAMP-only solution with those of other research groups (provided at the ICGEM website). EIGEN-CHAMP05S is a gravity field model made

at GFZ from six years of CHAMP GPS-SST and accelerometer data (10/2002–09/2008), Kaula regularization starts at degree 70 (Flechtner et al., 2010); AIUB-CHAMP03S is derived from eight years of GPS tracking data (2002–2009) using the celestial mechanics approach, no regularisation was applied (Jäggi et al., 2010). Especially on account of the decorrelation of the errors in GPS positions (Sect. 2.4), our model ASU-CHAMP-0309 performs almost as well as the AIUB-CHAMP03S model, below degree 20 both models are of comparable accuracy (note, however, that the AIUB-CHAMP03S model is based on one more year of data than our model). Besides our seven-year solution ASU-CHAMP-0309, we show also a six-year solution ASU-CHAMP-0308, based on GPS positions from the years 2003–2008; this solution performs better than EIGEN-CHAMP05S except for a few lowest degrees.

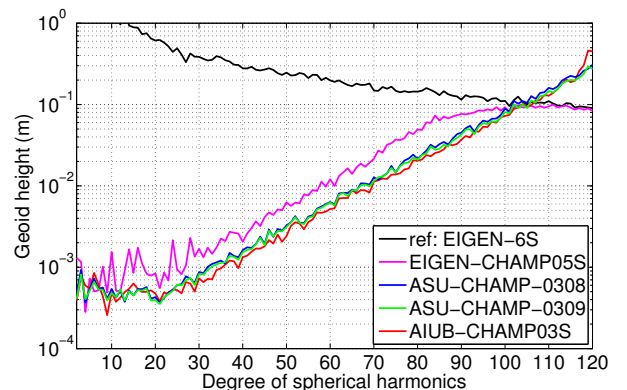


Figure 10: Degree difference amplitudes of four long-term CHAMP-only solutions.

### 3.7. Covariance matrices of GPS-SST solutions

In the upper panel of Fig. 11 we show the geographic distribution of the projected covariance matrix of one obtained solution in terms of geoid heights. A predominantly latitude-dependent (zonal) pattern, symmetric with respect to the equator, implies that the covariance matrix is approximately block-diagonal, if organized per spherical-harmonic order (Pavlis et al., 2012). This is due to the global, homogeneous sampling of GPS-SST data, as with the GRACE KBR models (Tapley et al., 2005). In the bottom panel of Fig. 11, among the lowest degree coefficients we see only moderate correlations (less than 0.54 in abs. value) for certain coefficients of the same order and same parity. We obtained similar results for all our yearly and multi-year solutions.

From Fig. 9 showing the agreement of our unconstrained long-term GPS-SST solutions with a KBR GRACE solution we can deduce a rule of thumb for ‘reasonable’ values of our fitted GPS-SST fields. Limiting the degree difference to be one tenth of that at the ‘crossing point’ with the reference field signal, we obtain the maximum degree 60 for the GRACE A/B and 75 for the CHAMP seven-year solutions. In such degree-limited solutions, 99.9 percent of correlations are less than 0.1 (in absolute value), all correlations are below 0.73 for the GRACE A/B solutions and below 0.61 for the CHAMP solution. Only the highest degree fitted coefficients have large correlations among themselves, but this is expected as they are included in the fit

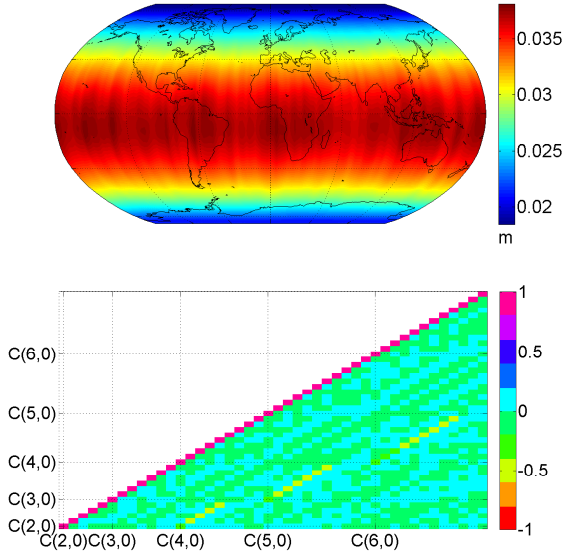


Figure 11: Geoid height error predicted by the full covariance matrix as a function of geographic location for the seven-year solution ASU-CHAMP-0309 up to degree 75; correlation matrix of the same solution up to degree 9, order of coefficients:  $C_{20}$ ,  $C_{21}$ ,  $S_{21}$ ,  $C_{22}$ ,  $S_{22}$ ,  $C_{30}$ , etc.

in order to reduce the truncation error and due to the degree-dependent altitude attenuation there is not enough information in the observations for them to be clearly separated. We recommend to exclude these highest degree estimated coefficients and their covariance information from further analysis; following this rule, the geographical map in the upper panel of Fig. 11 was computed from the seven-year solution ASU-CHAMP-0309 limited by maximum degree 75. Generally speaking, the covariance matrices of our solutions are diagonally dominant. This is in accordance with our experience that multi-year combination solutions (Sect. 3.6) are not much different when combining them by means of the full normal matrices or using only the elements on their main diagonals.

### 3.8. First results for GOCE

As mentioned in the introduction, in the GOCE mission the GPS-SST data constitute an important source of information complementary to the space gradiometer observations; the GPS positions are used to determine the long-wavelength part of the gravity field. In Fig. 12 we present our first attempts to compute the geopotential solution based on GPS-SST data from the first 2-month observation cycle. In the figure we also show one of the three official ESA solutions, so-called *time-wise solution*, whose aim is to be a pure GOCE-only solution independent of any prior gravity field model; its low-degree part is based on the energy integral method using the kinematic orbits (GO\_CONS\_GCF\_2\_TIM\_R1; Pail et al., 2011a). In the shown longwave part of this solution, Kaula regularization was applied to all zonal and selected near-zonal coefficients. Our solution ‘ASU-GOCE-2months’ display only slight deficiencies in the zonals due to the polar gap; this is because we selected not so high value of the maximum harmonic degree for the estimated coefficients ( $N=75$ ), and also owing to the combined information from all three LRF components (cf. Fig. 7). In the graphs

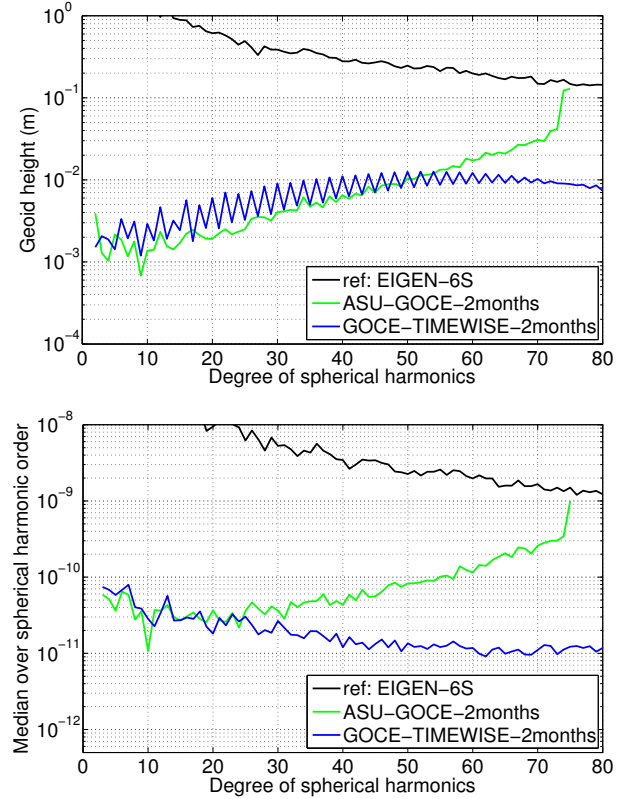


Figure 12: Degree difference amplitudes (upper panel) and degree medians (lower panel) of GOCE solutions. Data: Nov-Dec 2009.

of the ESA time-wise solution, SGG seems to be the dominant contributor in the combined solution from degree 30 onwards.

### 3.9. Time-variable gravity from GPS orbits

First attempts at revealing temporal variations in the CHAMP gravity fields (Sneeuw et al., 2005; Reigber et al., 2005a) were confronted with a large noise and have led to the conclusion that seasonal variations in only the lowest 2–4 harmonic degrees can possibly be recovered (Weigelt et al., 2009; Wang et al., 2012). Based on eight years of CHAMP GPS data, Prange et al. (2011) showed that it is possible to determine temporal gravity variations up to degree 10 by averaging and filtering the individual monthly solutions. Recently, Weigelt et al. (2013a) used a Kalman filtering to analyze non-stationary variations in the long-term trends and annual amplitudes of mass change over Greenland derived from GPS-SST data of CHAMP with a spatial resolution corresponding to degree and order 10.

We used CHAMP and GRACE A/B kinematic positions, for each satellite we fitted monthly solutions up to degree 20 within the period 2003–2009. To reduce the error due to the truncation of the geopotential harmonic series in Eq. (1), for each satellite before fitting the harmonic coefficients we subtracted the gravitational acceleration computed from its respective seven-year static solution, in case of GRACE A/B for degrees 21–80, in case of CHAMP for degrees 21–100 (Sect. 3.6). Thus the individual results on temporal variations are based solely on data from the satellite in question. Then we fitted a linear model consisting of the mean, trend and annual sinusoidal variations to the time

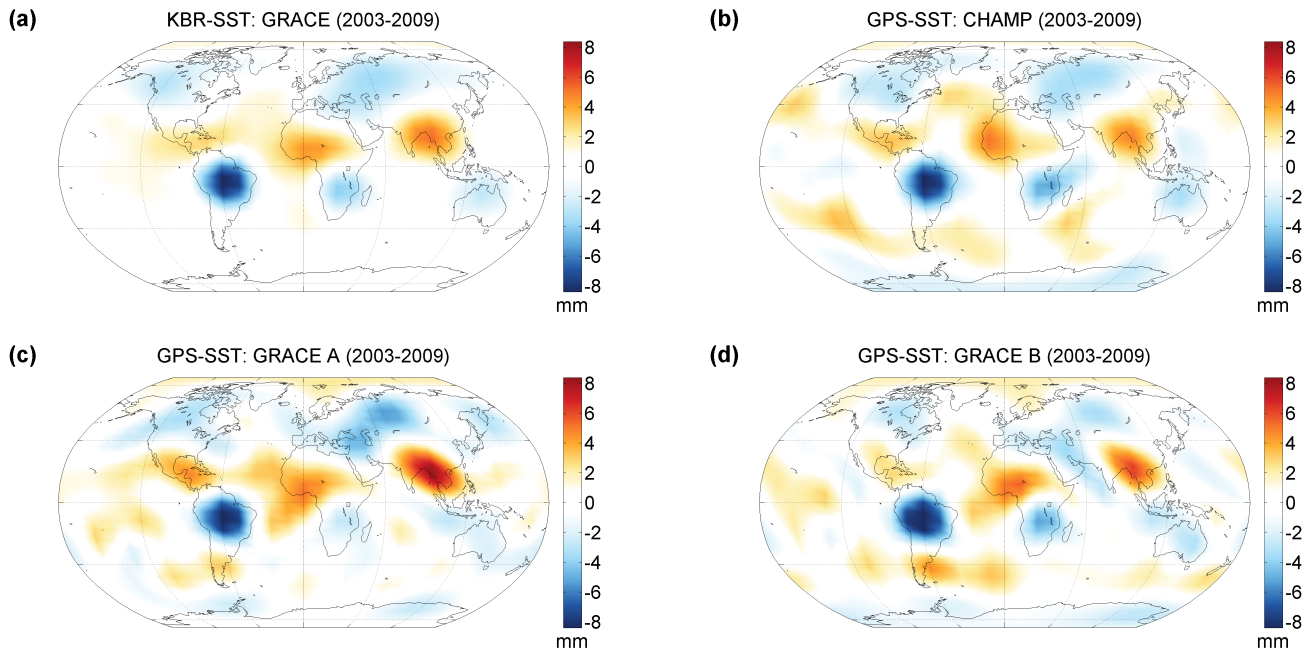


Figure 13: Average seasonal geopotential variation computed from: (a) GRACE KBR data (CSR RL04); (b)–(d) GPS positions of CHAMP, GRACE A/B satellites. In each map, average October variation in terms of geoid height is shown, maximum fitted harmonic degree is 10.

series of individual harmonic coefficients up to degree 10 (e.g. Wagner and McAdoo, 2004). In Fig. 13 we show geoid height maps of the obtained mean annual variations in panels (b)–(d). For comparison also a map for the annual change from GRACE KBR monthly solutions, computed in the same way, is given in panel (a). For the maps we chose the month of October when the gravity field seasonal cycle attains its extreme values. The averaged annual signal in all the four panels displays clearly the continental areas with most important hydrological variations. These include heavy-rainfall regions on both sides of the equator and a moderate seasonal signal in Eurasia and northern North America (Wahr, 2007). The GPS-SST average seasonal solutions (b)–(d) are noisier compared to the KBR field in panel (a); this is clearly visible over the oceans, where the annual variations are much smaller compared to those on land.

#### 4. Conclusions and outlook

Recent discussions about the capability of using GPS-only geopotential models for monitoring temporal variations of Earth gravity field are motivated by a possible gap between GRACE and its follow-on mission (Wang et al., 2012; Ditmar et al., 2009; Weigelt et al., 2013a). In this paper we presented an inversion method to compute the geopotential harmonic coefficients from GPS positions using the acceleration approach. We obtained static gravity field models up to degree 80–100 from high quality kinematic positions of low flying satellites GRACE A/B, CHAMP and GOCE equipped with GPS receivers. We demonstrated that the presented method yields long-term static CHAMP-only solution of similar or better quality as other published solutions. We showed that precise GPS positions of a single satellite may provide a realistic geographic pattern of average seasonal hydrology of continents.

The obtained results are encouraging and will serve as a basis for studying related problems, such as further refinement of the defining parameters of the presented method, especially for GOCE-like orbits; possibility of obtaining meaningful ‘non-average’ monthly solutions to provide more detailed time-variable gravity; combination of the GPS-SST solutions with solutions from other techniques (namely GOCE SGG).

#### Acknowledgements

Our sincere thanks are due to Adrian Jäggi (AIUB, Switzerland) for providing us with the kinematic orbits of CHAMP and GRACE satellites. Furthermore, the authors acknowledge ISDC/GFZ for other CHAMP and GRACE data; ESA for all the GOCE data; ICGEM/GFZ for the geopotential models, including the monthly solution time series. We thank Christian Siemes for useful comments. This work was supported by projects GA13-36843S, LH13071 and RVO: 67985815.

#### References

- Baur, O., Reubelt, T., Weigelt, M., Roth, M., Sneeuw, N. GOCE orbit analysis: Long-wavelength gravity field determination using the acceleration approach. *Advances in Space Research* 50, 385–396, 2012.
- Beutler, G., Jäggi, A., Mervart, L., Meyer, U. The celestial mechanics approach: application to data of the GRACE mission. *Journal of Geodesy* 84, 661–681, 2010a.
- Beutler, G., Jäggi, A., Mervart, L., Meyer, U. The celestial mechanics approach: theoretical foundations. *Journal of Geodesy* 84, 605–624, 2010b.
- Bezděk, A. Calibration of accelerometers aboard GRACE satellites by comparison with POD-based nongravitational accelerations. *Journal of Geodynamics* 50, 410–423, 2010.
- Bezděk, A., Klokočník, J., Kostelecký, J., Floberghagen, R., Gruber, C. Simulation of free fall and resonances in the GOCE mission. *Journal of Geodynamics* 48, 47–53, 2009.

- Bezděk, A., Sebera, J., Klokočník, J., Kostecký, J. Global gravity field models from the GPS positions of CHAMP, GRACE and GOCE satellites. In A. Abbasi, N. Giesen, editors, EGU General Assembly Conference Abstracts, volume 14 of EGU General Assembly Conference Abstracts, page 5980. 2012.
- Bock, H., Jäggi, A., Meyer, U., Visser, P., Ijssel, J., Helleputte, T., Heinze, M., Hugentobler, U. GPS-derived orbits for the GOCE satellite. *Journal of Geodesy* 85, 807–818, 2011.
- Brockwell, P., Davis, R. Introduction to Time Series and Forecasting. Lecture Notes in Statistics. Springer, 2002.
- Bruinsma, S., Thuillier, G., Barlier, F. The DTM-2000 empirical thermosphere model with new data assimilation and constraints at lower boundary: accuracy and properties. *Journal of Atmospheric and Solar-Terrestrial Physics* 65, 1053–1070, 2003.
- Cazenave, A., Chen, J. Time-variable gravity from space and present-day mass redistribution in the Earth system. *Earth and Planetary Science Letters* 298, 263–274, 2010.
- Chambers, D. P., Schröter, J. Measuring ocean mass variability from satellite gravimetry. *Journal of Geodynamics* 52, 333–343, 2011.
- Chatterjee, S., Hadi, A. S. Regression Analysis by Example. Wiley Series in Probability and Statistics. Wiley, 2006.
- Ditmar, P., Bezdek, A., Liu, X., Zhao, Q. On a Feasibility of Modeling Temporal Gravity Field Variations from Orbits of Non-dedicated Satellites. In Sideris, M G, editor, Observing our changing earth, volume 133 of International association of geodesy symposia, pages 307–313. Int Assoc Geodesy; Int Union Geodesy & Geophys, 2009. General Assembly of the International-Association-of-Geodesy/24th General Assembly of the International-Union-of-Geodesy-and-Geophysics, Perugia, ITALY, JUL 02-13, 2007.
- Ditmar, P., Klees, R., Liu, X. Frequency-dependent data weighting in global gravity field modeling from satellite data contaminated by non-stationary noise. *Journal of Geodesy* 81, 81–96, 2007.
- Ditmar, P., Kuznetsov, V., van der Sluijs, A. A. V. E., Schrama, E., Klees, R. 'DEOS\_CHAMP-01C.70': a model of the Earth's gravity field computed from accelerations of the CHAMP satellite. *Journal of Geodesy* 79, 586–601, 2006.
- Ditmar, P., Sluijs, A. A. V. E. D. A technique for modeling the Earth's gravity field on the basis of satellite accelerations. *Journal of Geodesy* 78, 12–33, 2004.
- EGG-C. GOCE Level 2 Product Data Handbook. GO-MA-HPFGS-0110, Issue 4.3. European Space Agency, 2010.
- ESA. Gravity Field and Steady-State Ocean Circulation Mission, report for mission selection of the four candidate Earth Explorer missions. ESA Report SP-1233(1). European Space Agency, 1999.
- ESA. Swarm The Earth's magnetic field and environment explorers. ESA Report SP-1279(6), 2004.
- Flechtner, F., Dahle, C., Neumayer, K. H., Koenig, R., Foerste, C. The Release 04 CHAMP and GRACE EIGEN Gravity Field Models. In Flechtner, F and Gruber, TH and Manda, M and Rothacher, M and Schone, T and Wickert, J, editor, System earth via geodetic-geophysical space techniques, Advanced Technologies in Earth Sciences, pages 41–58. Springer, 2010.
- Floborghagen, R., Fehring, M., Lamarre, D., Muzi, D., Frommknecht, B., Steiger, C., Piñero, J., da Costa, A. Mission design, operation and exploitation of the gravity field and steady-state ocean circulation explorer mission. *Journal of Geodesy* 85, 749–758, 2011.
- Földváry, L., Švehla, D., Gerlach, C., Wermuth, M., Gruber, T., Rummel, R., Rothacher, M., Frommknecht, B., Peters, T., Steigenberger, P. Gravity model TUM-2Sp based on the energy balance approach and kinematic CHAMP orbits. In C. Reigber, H. Lühr, P. Schwintzer, J. Wickert, editors, Earth Observation with CHAMP Results from Three Years in Orbit, page 13. Springer, 2005.
- Förste, C., Bruinsma, S. L., Shako, R., Abrikosov, O., Flechtner, F., Marty, J.-C., Lemoine, J.-M., Dahle, C., Neumeyer, H., Barthelmes, F., Biancale, R., Balmino, G., König, R. A new release of EIGEN-6: The latest combined global gravity field model including LAGEOS, GRACE and GOCE data from the collaboration of GFZ Potsdam and GRGS Toulouse. In A. Abbasi, N. Giesen, editors, EGU General Assembly Conference Abstracts, volume 14 of EGU General Assembly Conference Abstracts, page 2821. 2012.
- Götzelmann, M., Keller, W., Reubelt, T. Gross Error Compensation for Gravity Field Analysis Based on Kinematic Orbit Data. *Journal of Geodesy* 80, 184–198, 2006.
- Gray, R. M. Toeplitz and circulant matrices: A review. *Foundations and Trends in Communications and Information Theory* 2, 155–239, 2006.
- Gunter, B. C., Encarnação, J., Ditmar, P., Klees, R. Using Satellite Constellations for Improved Determination of Earth's Time-VARIABLE Gravity. *Journal of Spacecraft and Rockets* 48, 368–377, 2011.
- Hofmann-Wellenhopf, B., Lichtenegger, H., Wasle, E. GNSS - Global Navigation Satellite Systems. Springer, 2008.
- Holmes, S. A., Featherstone, W. E. A unified approach to the Clenshaw summation and the recursive computation of very high degree and order normalised associated Legendre functions. *Journal of Geodesy* 76, 279–299, 2002.
- Jäggi, A., Bock, H., Meyer, U. GPS-Only Gravity Field Recovery from GOCE. In 4th International GOCE User Workshop, volume 696 of ESA Special Publication. 2011a.
- Jäggi, A., Bock, H., Prange, L., Meyer, U., Beutler, G. GPS-only gravity field recovery with GOCE, CHAMP, and GRACE. *Advances in Space Research* 47, 1020–1028, 2011b.
- Jäggi, A., Dach, R., Montenbruck, O., Hugentobler, U., Bock, H., Beutler, G. Phase center modeling for LEO GPS receiver antennas and its impact on precise orbit determination. *Journal of Geodesy* 83, 1145–1162, 2009.
- Jäggi, A., Prange, L., Hugentobler, U. Impact of covariance information of kinematic positions on orbit reconstruction and gravity field recovery. *Advances in Space Research* 47, 1472–1479, 2011c.
- Jäggi, A., Prange, L., Meyer, U., Mervart, L., Beutler, G., Gruber, T., Dach, R., Pail, R. Gravity Field Determination at AIUB: From annual to multi-annual solutions. In EGU General Assembly Conference Abstracts, volume 12 of EGU General Assembly Conference Abstracts, page 5842. 2010.
- Klees, R., Ditmar, P., Broersen, P. How to handle colored observation noise in large least-squares problems. *Journal of Geodesy* 76, 629–640, 2003.
- Klokočník, J., Wagner, C. A., Kostecký, J., Bezděk, A., Novák, P., McAdoo, D. Variations in the accuracy of gravity recovery due to ground track variability: GRACE, CHAMP, and GOCE. *Journal of Geodesy* 82, 917–927, 2008.
- Lyard, F., Lefevre, F., Letellier, T., Francis, O. Modelling the global ocean tides: modern insights from FES2004. *Ocean Dynamics* 56, 394–415, 2006.
- Mayer-Gürr, T., Ilk, K. H., Eicker, A., Feuchtinger, M. ITG-CHAMP01: a CHAMP gravity field model from short kinematic arcs over a one-year observation period. *Journal of Geodesy* 78, 462–480, 2005.
- Mayer-Gürr, T., Kurtenbach, E., Eicker, A. ITG-Grace2010: the new GRACE gravity field release computed in Bonn. In EGU General Assembly Conference Abstracts, volume 12 of EGU General Assembly Conference Abstracts, page 2446. 2010.
- McCarthy, D. D. IERS Conventions (1996). IERS Technical Note 21, 1–95, 1996.
- Montenbruck, O., Gill, E. Satellite Orbits: Models, Methods, and Applications. Springer, 2000.
- Pail, R., Bruinsma, S., Migliaccio, F., Förste, C., Goiginger, H., Schuh, W.-D., Höck, E., Reguzzoni, M., Brockmann, J. M., Abrikosov, O., Veicherts, M., Fecher, T., Mayrhofer, R., Krasbutter, I., Sansò, F., Tscherning, C. C. First GOCE gravity field models derived by three different approaches. *Journal of Geodesy* 85, 819–843, 2011a.
- Pail, R., Goiginger, H., Schuh, W.-D., Höck, E., Brockmann, J. M., Fecher, T., Mayer-Gürr, T., Kusche, J., Jäggi, A., Prange, L., Rieser, D., Hausleitner, W., Maier, A., Krauss, S., Baur, O., Krasbutter, I., Gruber, T. Combination of GOCE Data with Complementary Gravity Field Information. In 4th International GOCE User Workshop, volume 696 of ESA Special Publication. 2011b.
- Pavlis, N. K., Holmes, S. A., Kenyon, S. C., Factor, J. K. The development and evaluation of the Earth Gravitational Model 2008 (EGM2008). *Journal of Geophysical Research (Solid Earth)* 117, B04406, 2012.
- Petit, G., Luzum, B., et al. IERS Conventions (2010). IERS Technical Note 36, 1, 2010.
- Prange, L. Global Gravity Field Determination Using the GPS Measurements Made Onboard the Low Earth Orbiting Satellite CHAMP. Ph.D. thesis, Astronomical Institute, University of Bern, Switzerland, 2010.
- Prange, L., Jäggi, A., Beutler, G., Dach, R., Mervart, L. Gravity Field Determination at the AIUB - The Celestial Mechanics Approach. In Sideris, M G, editor, OBSERVING OUR CHANGING EARTH, volume 133 of International Association of Geodesy Symposia, pages 353–362. Int Assoc Geodesy; Int Union Geodesy & Geophys, 2009. General Assembly of the International-Association-of-Geodesy/24th General Assembly of the International-Union-of-Geodesy-and-Geophysics, Perugia, ITALY, JUL 02-13, 2007.
- Prange, L., Jäggi, A., Dach, R., Bock, H., Beutler, G., Mervart, L. AIUB-CHAMP02S: The influence of GNSS model changes on gravity field recovery using spaceborne GPS. *Advances in Space Research* 45, 215–224, 2010.
- Prange, L., Meyer, U., Jäggi, A., Beutler, G. Temporal gravity field solutions at the AIUB. In EGU General Assembly Conference Abstracts, volume 13 of EGU General Assembly Conference Abstracts, page 6641. 2011.
- Press, W. M., Teukolsky, S. A., Vetterling, W. T., Flannery, B. P. Numerical recipes in Fortran 77. The Art of Scientific Computing. Cambridge University

- Press, 2001.
- Rawlings, J., Pantula, S., Dickey, D. Applied Regression Analysis: A Research Tool. Springer Texts in Statistics. Wadsworth & Brooks, 1998.
- Reigber, C., Jochmann, H., Wunsch, J., Petrovic, S., Schwintzer, P., Barthelmes, F., Neumayer, K.-H., König, R., Förste, C., Balmino, G., Biancale, R., Lemoine, J.-M., Loyer, S., Perosanz, F. Earth gravity field and seasonal variability from CHAMP. In C. Reigber, H. Lühr, P. Schwintzer, J. Wickert, editors, Earth Observation with CHAMP Results from Three Years in Orbit, page 25. Springer, 2005a.
- Reigber, C., Lühr, H., Schwintzer, P. CHAMP mission status. Advances in Space Research 30, 129–134, 2002.
- Reigber, C., Lühr, H., Schwintzer, P. First CHAMP Mission Results for Gravity, Magnetic and Atmospheric Studies. Springer, 2003b.
- Reigber, C., Lühr, H., Schwintzer, P., Wickert, J. Earth Observation with CHAMP Results from Three Years in Orbit. Springer, 2005b.
- Reigber, C., Schwintzer, P., Neumayer, K.-H., Barthelmes, F., König, R., Förste, C., Balmino, G., Biancale, R., Lemoine, J.-M., Loyer, S., Bruinsma, S., Perosanz, F., Fayard, T. The CHAMP-only earth gravity field model EIGEN-2. Advances in Space Research 31, 1883–1888, 2003a.
- Reubelt, T., Austen, G., Grafarend, E. W. Harmonic analysis of the Earth's gravitational field by means of semi-continuous ephemerides of a low Earth orbiting GPS-tracked satellite. Case study: CHAMP. Journal of Geodesy 77, 257–278, 2003.
- Reubelt, T., Baur, O., Weigelt, M., Roth, M., Sneeuw, N. GOCE long-wavelength gravity field recovery from high-low satellite-to-satellite-tracking using the acceleration approach. In A. Abbasi, N. Giesen, editors, EGU General Assembly Conference Abstracts, volume 14 of EGU General Assembly Conference Abstracts, page 4284. 2012.
- Reubelt, T., Götzelmann, M., Grafarend, E. W. Harmonic Analysis of the Earth's Gravitational Field from Kinematic CHAMP Orbits based on Numerically Derived Satellite Accelerations. In J. Flury, R. Rummel, C. Reigber, M. Rothacher, G. Boedecker, U. Schreiber, editors, Observation of the Earth System from Space, page 27. Springer, 2006.
- Rummel, R. Dedicated gravity field missions – principles and aims. Journal of Geodynamics 33, 3–20, 2002.
- Schäfer, C. Space Gravity Spectroscopy; The sensitivity analysis of GPS-tracked satellite missions (case study CHAMP). Ph.D. thesis, Geodätisches Institut der Universität Stuttgart, 2000.
- Schuh, W.-D. Tailored numerical solution strategies for the global determination of the earth's gravity field. Technical report, Number 81 in Mitteilungen der Universität Graz. Universität Graz., 1996.
- Sebera, J., Wagner, C. A., Bezděk, A., Klokočník, J. Short guide to direct gravitational field modelling with Hotine's equations. Journal of Geodesy 87, 223–238, 2013.
- Siemes, C. Digital Filtering Algorithms for Decorrelation within Large Least Squares Problems. Ph.D. thesis, University of Bonn, 2008.
- Sluijs, A. A. v. E. v. d. Inversion of satellite accelerations into the Earth's gravity field model. Master's thesis, Delft University of Technology, 2002. [http://www.lr.tudelft.nl/fileadmin/Faculteit/LR/Organisatie/Afdelingen.en.Leerstoelen/Afdeling\\_RS/Physical.and.Space.Geodesy/Publications/MSc\\_theses/doc/thesis.pdf](http://www.lr.tudelft.nl/fileadmin/Faculteit/LR/Organisatie/Afdelingen.en.Leerstoelen/Afdeling_RS/Physical.and.Space.Geodesy/Publications/MSc_theses/doc/thesis.pdf) [Online; accessed 29-Oct-2013].
- Sneeuw, N., Gerlach, C., Foldvary, L., Gruber, T., Peters, T., Rummel, R., Svehla, D. One year of time-variable CHAMP-only gravity field models using kinematic orbits. In Sanso, F, editor, WINDOW ON THE FUTURE OF GEODESY, volume 128 of International Association of Geodesy Symposia, pages 288–293. Int Assoc Geodesy, 2005. General Assembly of the International-Association-of-Geodesy, Sapporo, JAPAN, JUN 30-JUL 11, 2003.
- Sneeuw, N., van Gelderen, M. The polar gap. Lecture Notes in Earth Sciences, Berlin Springer Verlag 65, 559–568, 1997.
- Tapley, B., Ries, J., Bettadpur, S., Chambers, D., Cheng, M., Condi, F., Gunter, B., Kang, Z., Nagel, P., Pastor, R., Pekker, T., Poole, S., Wang, F. GGM02 An improved Earth gravity field model from GRACE. Journal of Geodesy 79, 467–478, 2005.
- Tapley, B., Ries, J., Bettadpur, S., Chambers, D., Cheng, M., Condi, F., Poole, S. The GGM03 Mean Earth Gravity Model from GRACE. AGU Fall Meeting Abstracts page A3, 2007.
- Tapley, B. D., Bettadpur, S., Watkins, M., Reigber, C. The gravity recovery and climate experiment: Mission overview and early results. Geophys. Res. Lett. 31, L09607, 2004.
- Švehla, D., Földvály, L. From Kinematic Orbit Determination to Derivation of Satellite Velocity and Gravity Field. In J. Flury, R. Rummel, C. Reigber, M. Rothacher, G. Boedecker, U. Schreiber, editors, Observation of the Earth System from Space, page 177. Springer, 2006.
- Švehla, D., Rothacher, M. Kinematic positioning of LEO and GPS satellites and IGS stations on the ground. Advances in Space Research 36, 376–381, 2005.
- Wagner, C. A., McAdoo, D. C. Time variations in the GRACE gravity field: Applications to global hydrologic mass flux. In Proceedings of the Joint CHAMP/GRACE Science Meeting. 2004.
- Wagner, C. A., McAdoo, D. C. Error calibration of geopotential harmonics in recent and past gravitational fields. Journal of Geodesy 86, 99–108, 2012.
- Wahr, J. Time variable gravity from satellites. In T. Herring, editor, Treatise on Geophysics, vol. 3, Geodesy, pages 213–237. Elsevier, 2007.
- Wang, X., Gerlach, C., Rummel, R. Time-variable gravity field from satellite constellations using the energy integral. Geophysical Journal International 190, 1507–1525, 2012.
- Weigelt, M. Global and local gravity field recovery from satellite-to-satellite tracking. Ph.D. thesis, University of Calgary, 2007.
- Weigelt, M., Baur, O., Reubelt, T., Sneeuw, N., Roth, M. Long Wavelength Gravity Field Determination from GOCE Using the Acceleration Approach. In 4th International GOCE User Workshop, volume 696 of ESA Special Publication. 2011.
- Weigelt, M., Dam, T., Jäggi, A., Prange, L., Tourian, M. J., Keller, W., Sneeuw, N. Time-variable gravity signal in Greenland revealed by high-low satellite-to-satellite tracking. Journal of Geophysical Research (Solid Earth) 118, 3848–3859, 2013a.
- Weigelt, M., Sideris, M. G., Sneeuw, N. On the influence of the ground track on the gravity field recovery from high-low satellite-to-satellite tracking missions: CHAMP monthly gravity field recovery using the energy balance approach revisited. Journal of Geodesy 83, 1131–1143, 2009.
- Weigelt, M., Sneeuw, N. Numerical Velocity Determination and Calibration Methods for CHAMP Using the Energy Balance Approach. In C. Jekeli, L. Bastos, J. Fernandes, editors, Gravity, Geoid and Space Missions, page 54. Springer, 2005.
- Weigelt, M., Sneeuw, N., Schrama, E. J. O., Visser, P. N. A. M. An improved sampling rule for mapping geopotential functions of a planet from a near polar orbit. Journal of Geodesy 87, 127–142, 2013b.
- Wermuth, M., Földvály, L., Svehla, D., Gerlach, C., Gruber, T., Frommknecht, B., Peters, T., Rothacher, M., Rummel, R., Steigenberger, P. Gravity Field Modelling From CHAMP Kinematic Orbits Using the Energy Balance Approach. In Proceedings of the Joint CHAMP/GRACE Science Meeting. 2004.
- Yi, W., Rummel, R. Contribution Analysis of the Gravity Field Recovered from GOCE. In 4th International GOCE User Workshop, volume 696 of ESA Special Publication. 2011.
- Zehentner, N., Mayer-Gürr, T., Mayrhofer, R. Gravity field determination using the acceleration approach - Considerations on numerical differentiation. In A. Abbasi, N. Giesen, editors, EGU General Assembly Conference Abstracts, volume 14 of EGU General Assembly Conference Abstracts, page 4713. 2012.